UNIVERSIDADE FEDERAL FLUMINENSE
INSTITUTO DE GEOCIÊNCIAS
DEPARTAMENTO DE GEOLOGIA E GEOFÍSICA

Geomagnetic Observations in Tatuoca: Data Processing and Temporal Characterization of the Equatorial Electrojet and Counter Electrojet

Gabriel Brando Soares

Projeto Final do Curso de Graduação em Geofísica

Niterói - RJ, Brasil
2017

GABRIEL BRANDO SOARES

Geomagnetic Observations in Tatuoca: Data Processing and Temporal Characterization of the Equatorial Electrojet and Counter Electrojet

Work presented to the Geophysics Bachelor Course of the Federal Fluminense University, as a requirement to obtain the degree of Bachelor in Geophysics.

Supervisors: Dra. Katia Jasbinschek dos Reis Pinheiro and Dr. Jürgen Matzka

Niterói - RJ, Brazil
2017

S676 Soares, Gabriel Brando
Geomagnetic Observations in Tatuoca: data processing and temporal characterization of the Equatorial Electrojet and Counter Electrojet / Gabriel Brando Soares. – Niterói : [s.n.], 2017.
66 f.

Trabalho de Conclusão de Curso (Bacharelado em Geofísica) – Universidade Federal Fluminense, 2017.

1.Geomagnetismo. 2.Processamento de dados magnéticos. 3.Observatório magnético. 4. Eletrojato Equatorial. I.Título.

CDD 538.7

GABRIEL BRANDO SOARES

Geomagnetic Observations in Tatuoca: Data Processing and Temporal Characterization of the Equatorial Electrojet and Counter Electrojet

Work presented to the Geophysics Bachelor Course of the Federal Fluminense University, as a requirement to obtain the degree of Bachelor in Geophysics.

EXAMINERS:

Dra. Katia Jasbinschek dos Reis Pinheiro - ON/MCTIC

Dr. Arthur Ayres Neto - UFF

Dr. Wagner Moreira Lupinacci - UFF

Niterói - RJ, Brazil
2017

Acknowledgements

Fortunately, many people and institutions helped me, direct or indirectly, to conclude my course and this work. First of all, I would like to thank my family. My parents, Flávio and Lícia, and my sister, Mariana, were always with me, in the best and worst moments of my bachelor course. Thanks for the love and for motivating me to study and learn all the time. Thanks for the unconditional support to develop my studies as best as possible. I deeply thank Sueli for taking care of me and my family since I was born.

I am very grateful to my supervisor and great friend, Dr. Katia Pinheiro, who accepted me as a student since my third period when I did not have any idea of how to work with geomagnetism. During this time she taught me more than science and all the opportunities that I had in my course are consequences of the door opened by her in 2013. Thanks for carefully guiding me and for the constant motivation.

I would like to thank very much Dr. Jürgen Matzka from GFZ-Potsdam for supervising me in this final project and in our cooperation project. I am very grateful for having his broad knowledge about magnetic observatories and geomagnetism shared with me. I have never learned so many things in a short period of time like I did during my visit in Niemegk. Thanks for all unique opportunities given to me.

Further, I want to thank Achim Morschhauser for all his valuable tips during some challenges with MATLAB, GMT and about my academic career. I thank Carlos Veiga for his indispensable help with the program to calculate sunrise and sunset times with accuracy. As well, I am grateful to Márcia Polck, who initiated me, very carefully, into the academic world, giving value to my work.

In addition, I want to thank Dr. Arthur Ayres for accepting the invitation to be one examiner of this work and for helping me with so many questions and details during the end of my course. I also thank Dr. Wagner Lupinacci for the positive answer to be an examiner of my final project.

I want to thank my great friends from the bachelor course: Lucas Eugenio, Matheus Lima and Reinaldo Mozart. We did almost all steps in the University together and I am certain that each subject would be much more difficult without their help. We learnt a lot together, but we were together in the funniest moments of our lives too.

I also would like to acknowledge the institutions that allowed me to construct my career in geosciences. Thanks UFF for providing the geophysics course and the teachers of the Geology and Geophysics Department, which taught me so many fundamental concepts. I thank Observatório Nacional for the opportunities as an intern and as a scientific initiation student, where I participated in field works and developed my research projects. Besides, I thank GFZ-Potsdam as well, for accepting me as a trainee in the Adolf-Schmidt Observatory. I am thankful for SBGf and Museum of Earth Sciences (CPRM) for the two years of internship and apprenticeship.

A special acknowledgement to my dear Laís, my great company, who teaches me how to have a happy life. I thank for her support and for the patience during all this hard work. Herr dedication and kindness have been extremely important in my life.

Abstract

The Tatuoca Magnetic Observatory (PA-Brazil) have been operating on an island in the Amazon River since 1957. This observatory plays an important role as a place where long term and accurate geomagnetic observations on the Brazilian equatorial margin are made. This work aims to produce calibrated data from the period of June 2008 to January 2016 of Tatuoca records and update one long period of unprocessed data, allowing its interpretation and future research. Since Tatuoca Observatory is set close to the magnetic equator (a dynamic feature, which changes with time), its records show how Tatuoca changed from one magnetic hemisphere to another and how the Equatorial Electrojet current system affects its signal, producing features such as the Counter Electrojet. To perform a detailed investigation of the Tatuoca magnetic signal, a comparison with the nearby Kourou Observatory (French Guiana) was done. In this work, I also present the applications of magnetic data from observatories and satellite missions in several activities, as in the oil industry. The final project is a result of an international cooperation established between the National Observatory (Brazil) and GFZ Potsdam (Germany).

Key words: Geomagnetism; Magnetic Observatories; Equatorial Electrojet; Magnetic Data Processing.

Resumo

O Observatório Magnético de Tatuoca (PA - Brasil) funciona em uma ilha situada no Rio Amazonas, desde 1957. Tal Observatório desempenha a importante função de realizar observações geomagnéticas contínuas e de alta precisão na margem equatorial brasileira. Esse trabalho tem como motivação a produção de dados calibrados referentes ao período entre junho de 2008 a janeiro de 2016 das observações em Tatuoca e, desta forma, preencher uma significativa lacuna de dados sem processamento, o que permitirá uma posterior interpretação e desenvolvimento de pesquisas com esse novo conjunto de dados. Como o Observatório de Tatuoca está localizado na região do equador geomagnético (feição dinâmica que varia com o tempo), seus registros apresentam como Tatuoca mudou de hemisfério magnético e como o sistema de correntes ionosféricas do Eletrojato Equatorial afeta o seu sinal, produzindo feições como o Contra-Eletrojato. Para realizar uma investigação detalhada do sinal magnético observado em Tatuoca, uma comparação com o Observatório de Kourou (Guiana Francesa) foi feita. Informações adicionais sobre as aplicações dos dados de observatórios magnéticos e missões de satélites em diversas atividades, como a indústria do petróleo, também serão abordadas. Esse projeto final resulta de uma cooperação internacional estabelecida entre o Observatório Nacional (Brasil) e o GFZ-Potsdam (Alemanha).

Palavras-chave: Geomagnetismo; Observatórios Magnéticos; Eletrojato Equatorial; Processamento de dados magnéticos.

Contents

List of Figures

List of Tables

List of Abbreviations

BGS .... British Geological Service
CEJ .... Counter Electrojet
EEJ .... Equatorial Electrojet
ECEJ .... Evening Counter Electrojet
ETT .... Etaiyapuram Magnetic Observatory
HYB .... Hyderabad Magnetic Observatory
IGRF .... International Geomagnetic Reference Field
KOU .... Kourou Magnetic Observatory
MCEJ .... Morning Counter Electrojet
PA .... State of Pará, Brazil
PNL .... Pantanal Magnetic Observatory
SAMA .... South Atlantic Magnetic Anomaly
TTB .... Tatuoca Magnetic Observatory
VSS .... Vassouras Magnetic Observatory

1 Introduction

The observed magnetic field of the Earth is a result of contributions from several sources that differ in nature and location. The main source of the geomagnetic field is on the dynamics of the electrically conductive fluid in the outer core (main internal source). Other internal sources are the lithospheric and the induced fields. There are also sources in the near-Earth space environment caused by electric current systems in the ionosphere and magnetosphere[1]. Fig. 1 shows the spatial distribution of the mentioned sources and the principal modalities of magnetic field observation: ground observatories and satellites.

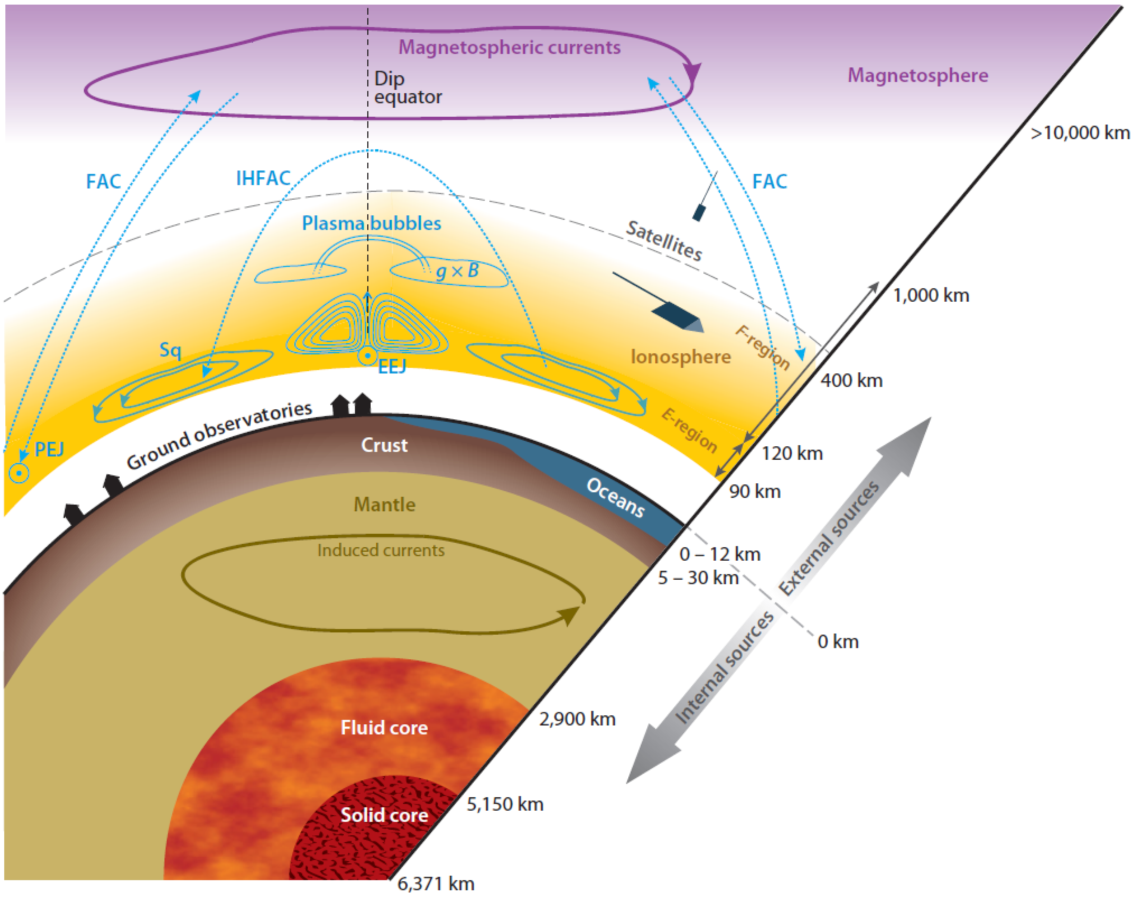

Figure 1: Sketch of the main sources (internal and external) which contributes to the Earth's magnetic field. Abbreviations: B, ambient magnetic field; EEJ, equatorial electrojet; FAC, field-aligned current; g, Earth's gravity vector; IHFAC, interhemispheric field-aligned current; PEJ, polar electrojet; Sq, solar quiet daily magnetic variation. Taken from Olsen and Stolle (2012).

The internal sources are generated and maintained in the planet's interior. The

[1]The ionosphere is the region, at Earth, of heights between 80 km and 1500 km and the magnetosphere is located about 10 to 12 Earth radii and it is the region around the Earth where its magnetic field is confined.

main component of the geomagnetic field (called the main field) is produced by convection in Earth's metallic liquid outer core (Amit, 2014), known as the self-sustaining geodynamo process (Fig. 2) that produces the longest time variations of Earth's magnetic field. The core field may be approximated by a tilted dipole, but it has also multipolar terms. The core field is by far the most intense contribution, on the order of 30000 nT at the equator and 60000 nT at the poles and corresponds to 90% of the observed field.

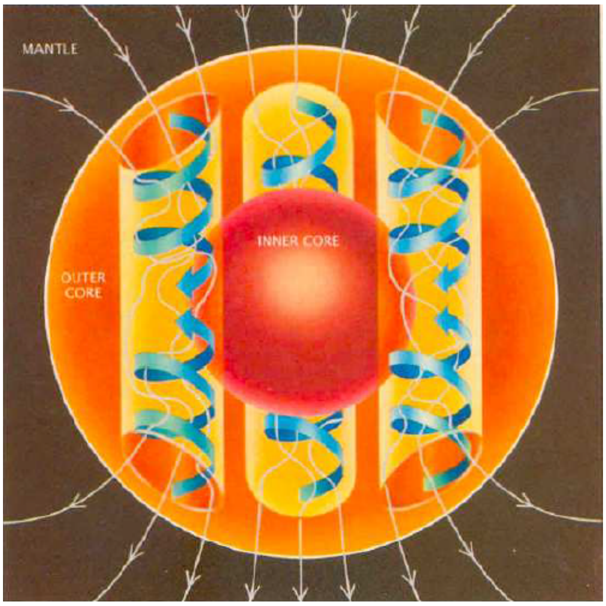

(a)

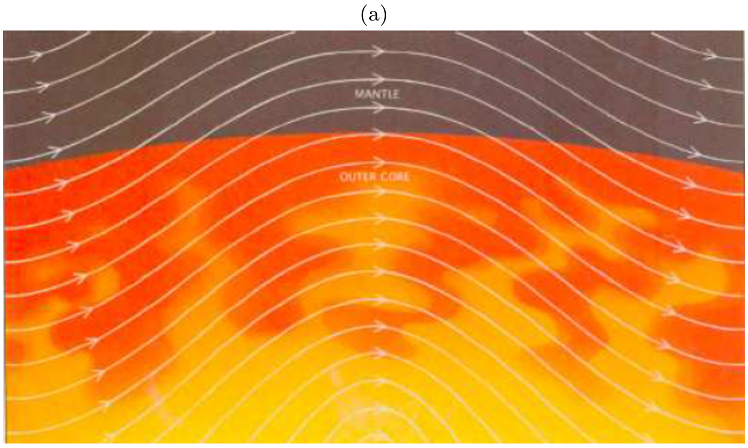

(b)

Figure 2: The mechanisms of the geodynamo in a planetary overview (a), where the blue arrows indicate the movement of the liquid and the white lines correspond to those of the magnetic field, and focusing in the core-mantle boundary (b), in which a region with higher temperatures in the outer core, causes an ascension of its electrically conductive fluid and, hence, deviating the lines of the magnetic field. Taken from Bloxham and Gubbins (1988).

The crustal or lithosphere field is caused by the magnetized rocks of the crust and changes substantially as function of location, depending on the geological history and concentration of magnetic rocks, whereas the induced field is generated by the conductive mantle and oceans due to external fields variations.

The planetary environment sources, also termed as external field (Fig. 3), consists of the interaction of Earth's main magnetic field with fields transported by the solar wind. Electrons and ionized hydrogen and helium (plasma) flows to all directions from the solar corona (Sun's outer layer), constituting the solar wind. The external fields are a result of the interaction of the ionospheric and magnetospheric plasmas with the solar wind that generates electrical currents and, hence, additional magnetic fields (Baumjohann et al., 2010).

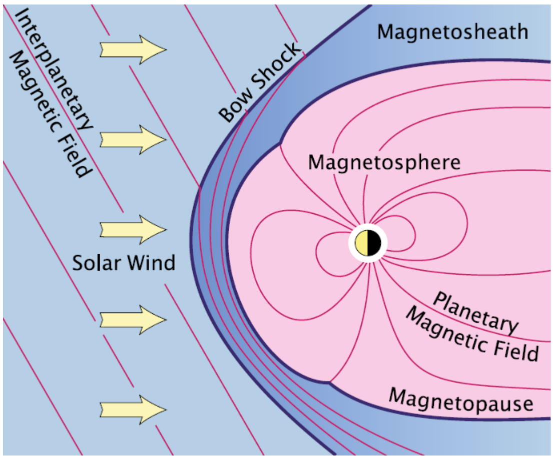

Figure 3: External magnetic field of a planet: interaction of the solar wind with the planetary field. Taken from Baumjohann et al. (2010).

1.1 Magnetic Field Components

The Earth's magnetic field is a vector, i.e., it has magnitude and direction. The magnitude of the field (F) is measured in the unit *Tesla* (T). However, one tesla is extremely strong when compared with the intensity of Earth's field. So, in this sense, the unit 10^{-9}T or nanotesla (nT) is adopted in geophysics as the practical unit for expressing the intensity of the geomagnetic field.

The magnetic vector may be expressed in Cartesian coordinates by X, Y and Z or in spherical polar coordinates by F, D and I elements (Lowrie, 2007). The geomagnetic components are shown in Fig. 4 in relation to the geographic north and east and the vertical directions. The direction of the total field intensity (F) is specified by two angles: the declination D, the angle between the magnetic north and geographic north, and the inclination I, the angle at which the magnetic vector dips below the horizontal. It is possible to obtain the following relations between the Earth's magnetic field components:

$$
\begin{aligned}
H &= F\cos(I), & X &= H\cos(D), \\
Y &= H\sin(D), & Z &= F\sin(I), \\
F^2 &= X^2 + Y^2 + Z^2, & H^2 &= X^2 + Y^2.
\end{aligned} \tag{1}
$$

The geomagnetic charts for the total intensity, declination and inclination in 2015 are shown in Fig. 5, using the reference model of Earth's magnetic field IGRF (12th version). It is interesting to note how the total intensity varies spatially (Fig. 5a) and how D and I control its direction on the globe (Figs. 5b - 5c). The South Atlantic Magnetic Anomaly (SAMA) is the region of lowest intensity of the magnetic field, as indicated by the arrow in Fig. 5a.

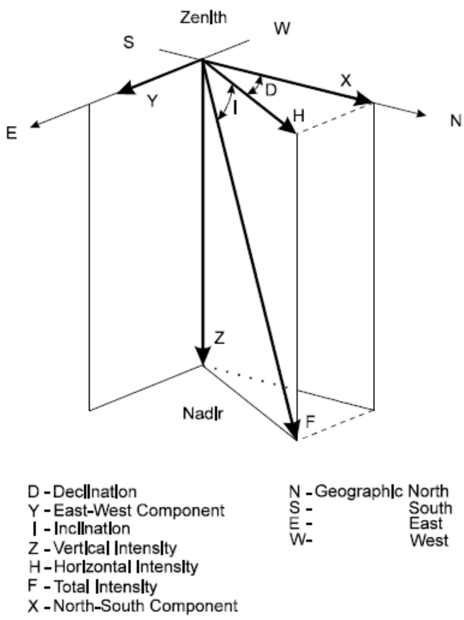

Figure 4: Geomagnetic field components. Taken from St-Louis (2011).

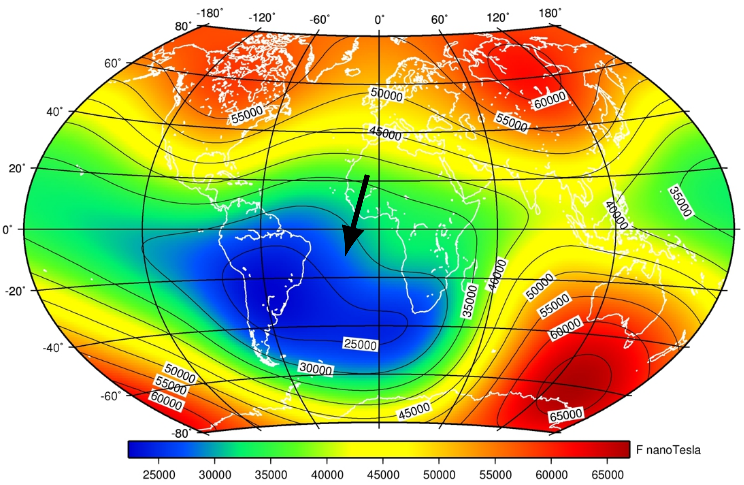

(a)

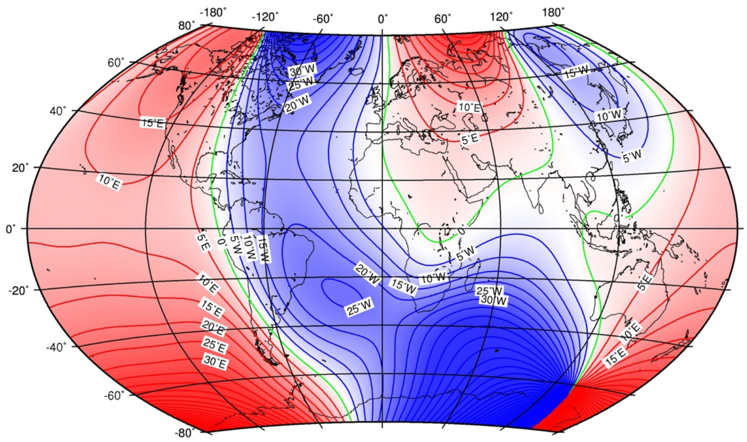

(b)

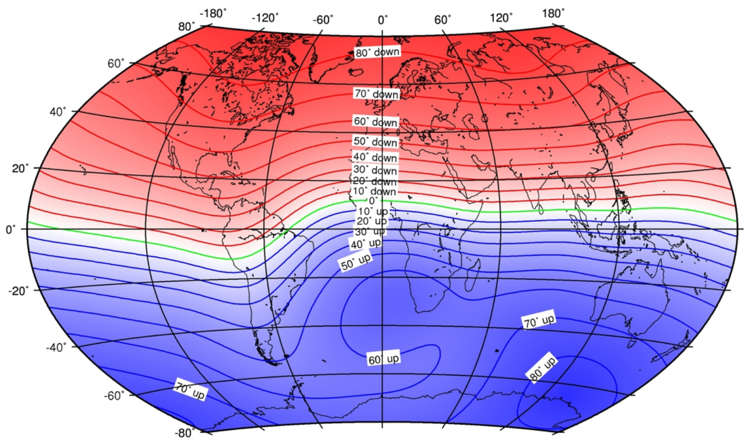

(c)

Figure 5: Global maps of the total field (a), declination (b) and inclination (c) for 2015 using the 12th International Geomagnetic Reference Field (IGRF). Produced by BGS (British Geological Survey).

1.2 Temporal Variations

The geomagnetic field changes in time from milliseconds to millions of years. Roughly, it is possible to consider two main types of variations: those with origin associated to the internal field and those related to the external field. Core field variations range from a few months to millions of years , due to changes in Earth's interior dynamics. Such gradual and slow changes constitute a classification of field variation, known as secular variation (Figures 6 and 7) . However the temporal fluctuations associated to the external field range from milliseconds to a few decades.

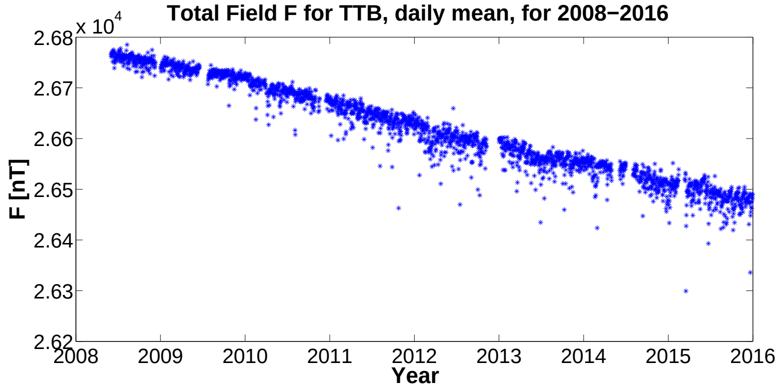

Figure 6: Slow decrease of the total field measured in Tatuoca Observatory, from 2008 to 2016. Such field variation corresponds to the secular variation.

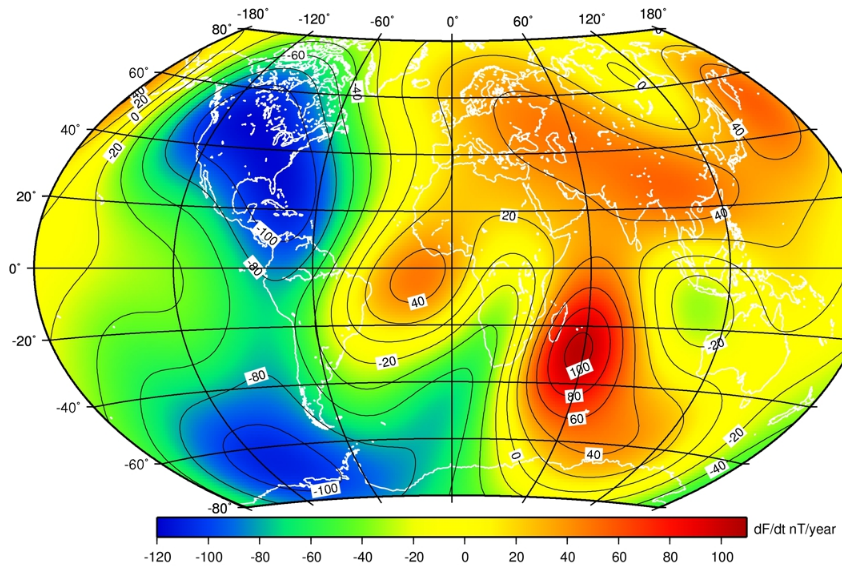

Figure 7: Global map of the secular variation of F for the period 2015-2020. Future values of the magnetic field are predicted by models like the IGRF. Produced by BGS.

Regarding the main external field variations, there are regular events, as daily variations related to the ionization of the dayside ionosphere (100-130 km of heigh in the atmosphere) heated by the Sun and, there are irregular events, such as magnetic storms produced by abrupt ejections of plasma from the Sun that pushes the Earth's magnetosphere (Love, 2008). Fig. 8 shows an example of a magnetic storm on the H component at Tatuoca Observatory (Brazil) and its sudden commencement is visible just before 21h of day 4, indicated by the red arrow. Before this event there is a solar-quiet (Sq) period and, after, a solar-disturbed (Sd) period due to the storm.

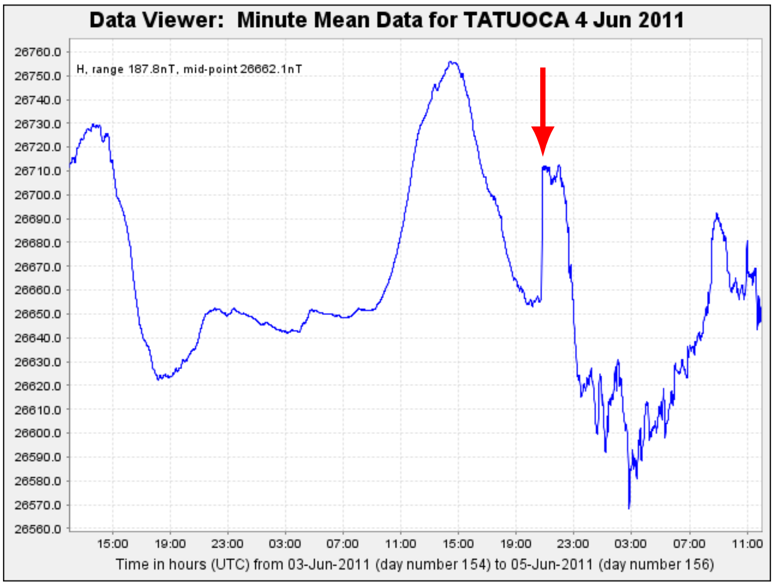

Figure 8: Time variation of the horizontal component (H) of Tatuoca Observatory, from 03-Jun-2011 12:00 to 05-Jun-2011 12:00 (time in UTC). Data was loaded in INTERMAGNET IMCDView data viewer.

1.3 The Equatorial Electrojet and Counter Electrojet

The Equatorial Electrojet (EEJ) is an equatorial current system along the magnetic equator (Fig. 9) within a narrow band of about 2°latitude, located at about 105 km height (Carvalho et al., 2010). This electrical current system points eastwards, moves with the Sun from east to west and produces an associated magnetic field. Its magnetic field intensity at the Earth's surface ranges up to about 100nT directed horizontally northward, leading to an enhancement of the horizontal component of the field.

The EEJ is caused by the sum of several factors like natural current systems due to daily tidal motion of the atmosphere (Sq current[2]), to the special geometry

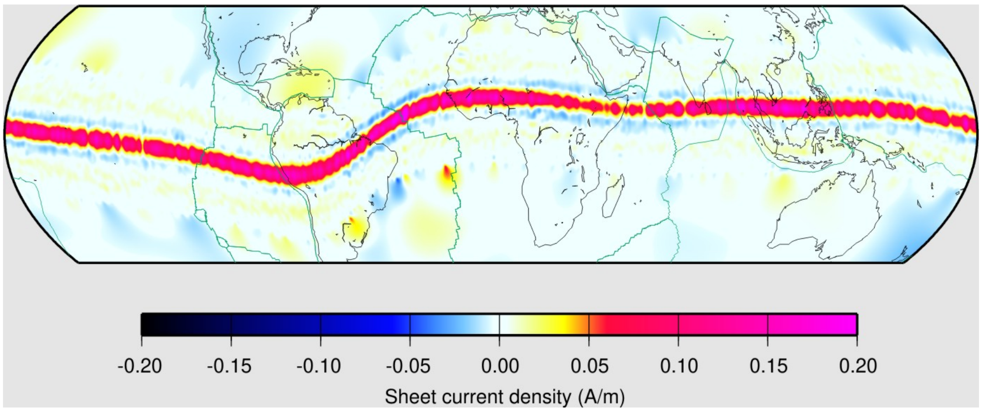

Figure 9: EEJ current densities inferred from CHAMP satellite mission data, between 11h and 13h local time. Taken from http://geomag.org/info/equatorial_electrojet.html

of the magnetic field at the equator (it is horizontal) and further supported by the nearly perpendicular incidence of solar radiation, which strongly enhance the effective conductivity (Baumjohann and Nakamura, 2007).

Occasionally, the EEJ appears to reverse into a westward Counter Electrojet (CEJ), defined as a decrease in the horizontal intensity of the equatorial field, for a period of few hours, in occasions at the morning and/or evening. This phenomena have been credited to the existence of an oppositely directed current in the EEJ region of the ionosphere (Campbell, 1997). The definitions of EEJ and CEJ will be very important during this work.

1.4 Open Questions in Geomagnetism

Many fundamental questions in geomagnetism are still under debate, for example:

(i) It is not entirely understood how the geomagnetic field behaves during the process of reversals and why the intervals of reversals are irregular.

(ii) The origin and the future of SAMA is still unknown.

(iii) The lower mantle electrical conductivity is a big question in geomagnetism. The assemblage of mineral physics, induction and seismological studies gives a clue on this topic. The interaction of the core field with the lower mantle is a fundamental question (Pinheiro, 2009).

[2] This current system causes the solar quiet variation/quiet daily variation.

1.5 Applications

In addition to the better understanding of Earth's dynamics, geomagnetism is, essentially, a branch of geophysics that is often applied to various activities, such as the oil industry, magnetic surveys, satellite operations, investigation of induction in electric power grids and long pipelines, global positioning system and navigation.

1.5.1 Mineral and Oil Industries

Magnetic surveys investigate local or regional geology through the analysis of the anomalies obtained in the measured magnetic field, which results from the magnetic properties of the underlying rocks. These surveys can be performed on land, at sea and in the air. This technique is widely employed for searching types of ore deposit that contain magnetic minerals (Kearey et al., 2002). In this sense, magnetic anomalies caused by rocks are superimposed on the total geomagnetic field (Fig. 10). Thus, knowing about the global geomagnetic field at a given place (or models, like IGRF) is fundamental both for the reduction of magnetic data to a suitable datum and for the interpretation of the resulting anomalies.

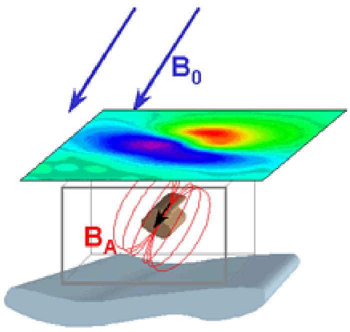

Figure 10: Schematic example of an observed field, which results from a superposition of Earth's field (B_0) and the field of a subsurface body (B_A). Taken from https://www.eoas.ubc.ca/research/ubcgif/iag/methods/meth_3/index.htm

Magnetometry is also useful for the oil industry, usually before a seismic survey, to provide regional magnetic data of the studied area. In this context, data from nearby observatories are used for the temporal reduction of the survey.

Navigating towards underground targets when drilling for oil and gas is a challenging task: in some areas, target sizes are small and there is an increased risk of collision with existing wells in the subsurface (Fig. 11). These targets demand a directional drilling of very long wells that rely on accurate models of the Earth's magnetic field that consider its time variation. The geomagnetic field models used in the hydrocarbon industry are computed from data collected by ground-based magnetic observatories network and from satellite missions (Beggan et al., 2014).

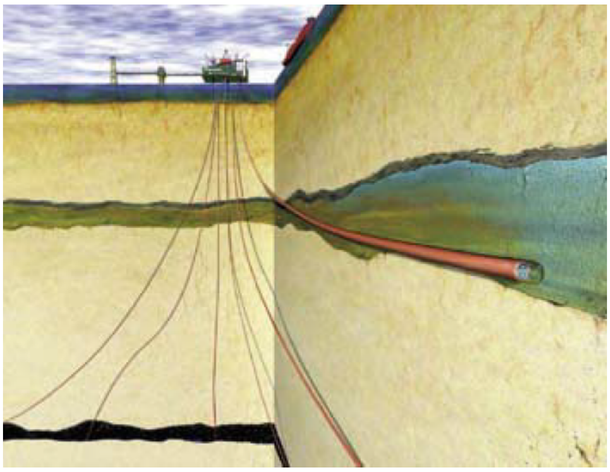

Figure 11: Illustration of complex horizontal drilling through underground. Taken from Beggan et al. (2014).

Magnetic data from observatories and other measurements are also applied in the oil industry, especially in its directional drilling techniques. Directional drilling is a firmly established technique in use within the oil industry to drill and allow wellbores to reach the targets. Using magnetic survey instruments to make measurements while drilling (MWD), allows to reduce the operational costs and drilling time. Therefore, high quality information on the Earth's magnetic field is needed to obtain the required levels of accuracy for MWD magnetic surveys (in Fig. 12, green and red lines are badly and nicely corrected well paths, respectively).

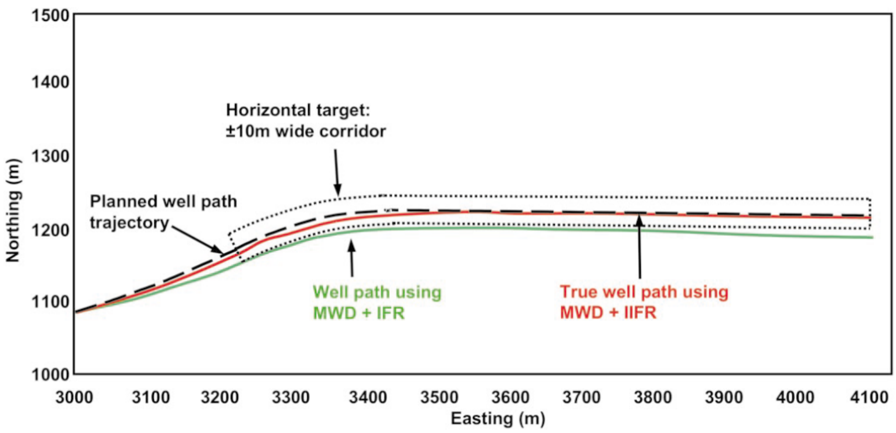

Figure 12: Examples of a horizontal well path where the planned path (dashed line) needed to reach the horizontal target (±10 m wide corridor). Taken from: Reay et al. (2005).

1.5.2 Space Weather Effects

The solar-terrestrial environment in which satellites are orbiting the Earth is a source of potential risks for the operation of such missions. For example, on-board computers in space systems have their lifetimes affected by the amount of radiation damage, caused by magnetospheric particles, to their circuitry. This environment can also determine the efficiency of solar-cell arrays of satellites during the years of operation. Additionally, thermospheric winds and density changes can cause transitory tracking loss and eventually shorten satellite lifetimes. In occasions of intense solar-terrestrial disturbance activity, satellites can be completely disabled (Campbell, 1997).

Fluctuations of the geomagnetic field due to ionospheric currents or, even, magnetic storms, are responsible for induction of currents along pipelines causing pipe corrosion (Silbergleit, 2015) that can also occur near the magnetic equator where stronger induced currents arise from the EEJ. Damaging currents induced in power grids may cause power blackouts of cities and consequent adversities (Beggan et al., 2013) as well as errors of several tens of meters in positions determined by Global Positioning Systems (Rao et al., 2009) due to propagation delays of its signals in the disturbed ionosphere (Fig. 13).

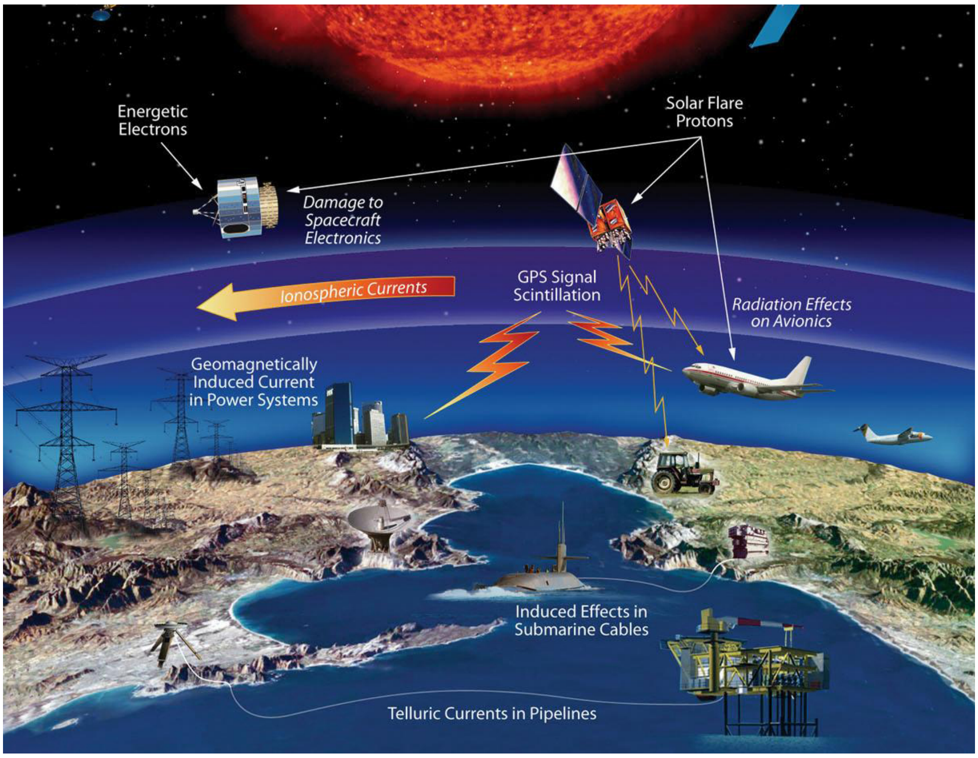

Figure 13: Illustration of technologies and infrastructure affected by space weather events. Credits: NASA.

To avoid these undesired and prejudicial effects in such activities, space weather forecasts (based on global observatory network data) and geomagnetic indices are developed to warn about space environment activity levels.

1.5.3 Navigation

Positioning through magnetic directions (as in the use of compass) and charts for navigation have been practice for a long time. Nowadays, some aircraft and ships still depend on the simple magnetic compass and charts for navigation. Information about the local magnetic declination is, still, very common throughout the world. Thus, geomagnetic data and charts continue to be valuable and necessary for navigation.

1.6 Objectives

The main goal of this work is to prepare, process and interpret the dataset from the period of June 2008 until January 2016 of magnetic measurements in the Tatuoca Magnetic Observatory (TTB, Pará - Brazil), comparing it with one dataset from the nearby Magnetic Observatory of Kourou (KOU, French Guiana). Such comparison is motivated by the demonstration of some interesting features of the geomagnetic field at this region, as the crossing of the magnetic equator, the equatorial electrojet and counter electrojet. All these peculiarities are well represented and documented by TTB records, what makes this location a very interesting location to monitor the Earth's magnetic field.

An extra motivation for this work is the recent modernization of TTB (November 2015), with new equipment and data transmission. The goal is to include TTB in the global network of magnetic observatories (INTERMAGNET). Another intention is to demonstrate how TTB data can be useful to be applied in the industry and some other human activities.

The main questions and subjects to be discussed in this project are:

(i) Which are the effects of EEJ and CEJ in TTB and KOU datasets? How these signals vary along the seasons?

(ii) How reliable is our detection of CEJ events? How is the relation between the signal of a CEJ and the sunrise and sunset times for a given place?

(iii) How often is the occurrence of CEJs in the area of study? How are these CEJs distributed during the days (morning or evening) and the year (along the seasons)?

The following sections will explain the fundamentals of magnetic measurements and observatories (section 2), how the data was chosen, prepared and which techniques were applied (section 3) to obtain the final results (section 4), considering the chronological order of each step.

2 Magnetic Measurements

Although geomagnetic data is very important for many applications, it is very challenging to cover uniformly the Earth's surface with accurate and high-quality data. To provide good spatial data coverage, there are different kinds of measurements, such as magnetic observatories, marine, aircraft and satellite surveys. This work only analyses magnetic data from surface observatories.

A complete description of the geomagnetic field requires at least independent measurements of three components, as seen in Section 1.1. Unfortunately, magnetometers can not measure the contributions of each source separately, but the final resulting field. The separation of different sources is performed by using a mathematical method, known as spherical harmonic analysis. Data in a good spatial and temporal resolutions are fundamental to get a good representation of the magnetic field in the globe.

A summary of the main magnetic field observations and surveys is listed below:

(i) Magnetic Observatories: fixed places at the Earth's surface where the geomagnetic field vector is recorded continuously over a long period of time. For example, the oldest observatories have been working for more than 100 years, such as Alibag (India, 1904), Eskdalemuir (United Kingdom, 1908) and Vassouras (Brazil, 1915) observatories. Worldwide magnetic observatories activities are coordinated by IAGA (International Association of Geomagnetism and Aeronomy) and INTERMAGNET (International Real-time Magnetic Observatory Network), which set the quality patterns, formats and transmission of data. In this work I only use data from magnetic observatories.

(ii) Magnetic Satellite Missions: observations of Earth's magnetic field from satellites moving in a Low Earth Orbit (LEO[3]). Usually these missions measure only field variations, but there is a minority of dedicated missions where the magnetic field is measured absolutely.

(iii) Repeat Stations: site whose position is known with high precision and where accurate absolute measurements of the geomagnetic field vector are made at regular intervals of typically two to five years between repeat station occupations, in order to provide information about long term variations, as the secular variation of Earth's magnetic field. The repeat stations are used as a complement to the observatories. They are very useful in large countries as Brazil, where it is difficult to provide a good observatory data coverage.

[3] The Low Earth Orbit (LEO) is defined as a spherical region that extends from the Earth's surface up to an altitude of 2000 km (definition of IADC Space Debris Mitigation Guidelines, 2007). A satellite in a LEO moves at approximately 8 km/s.

(iv) Aeromagnetic and Marine Surveys: magnetic surveys through aircraft or ships applied to the study of the field generated in the Earth's lithosphere, which can, for example, indicate the concentration of magnetic minerals and, hence, economically interesting mineral deposits.

2.1 Magnetic Observatories

An observatory must be placed in a suitable chosen location, where there are no artificial magnetic field disturbances that would contaminate the records and, ideally, free of crustal magnetic anomalies (Matzka et al., 2010). In this case, magnetometers must record continuously the natural field varying with time. Basically, two different types of instruments are used in an observatory: the absolute magnetometer and the variometer. The absolute scalar magnetometer is used, together with a DIflux magnetometer attached to a theodolite, to provide the absolute measurements of an observatory (performed manually by an operator, weekly), which establishes its variometer's baseline (reference) values. The variometer measures, as an automatic station, continuously the variation of the field components in relation to its baseline values. Both instruments are necessary in an observatory, because the definitive data is only produced once data from these two types of magnetic field measurement are obtained.

The importance of knowing the baseline values is justified for two main reasons: 1) it provides, immediately, the quality of the produced data and shows how stable it is, through a visual analysis (baseline plots); 2) with the baseline values, it is possible to obtain the definitive data of a magnetic observatory. Basically, the baseline can be considered as an interpolation of the available absolute measurements. In addition, as the offset of a variometer is adopted in an arbitrary way, the baseline valus doesn't have a physical meaning. Fig. 14 shows examples of baselines for the H, D and Z components of Vassouras Magnetic Observatory (VSS) in 2008, in which smooth and stable baselines are observed.

Matzka et al. (2010) presented what is considered as the minimum outfit for a magnetic observatory:

(i) At least two buildings: the variometer hut and absolute hut, both placed distant from artificial magnetic disturbances (Fig. 15).

(ii) A set of absolute instruments is kept on pillars in the absolute hut. An azimuth mark in a distance greater than 100 m is necessary for the absolute observations procedures and must be visible from the pillars (Figs. 16a - 16b).

(iii) A variometer is kept inside the variometer hut on a stable pillar at constant temperature (Fig. 16c).

(iv) Additional equipment (such as data logger, computers and power supply) is often necessary in nearby buildings (Fig. 16d).

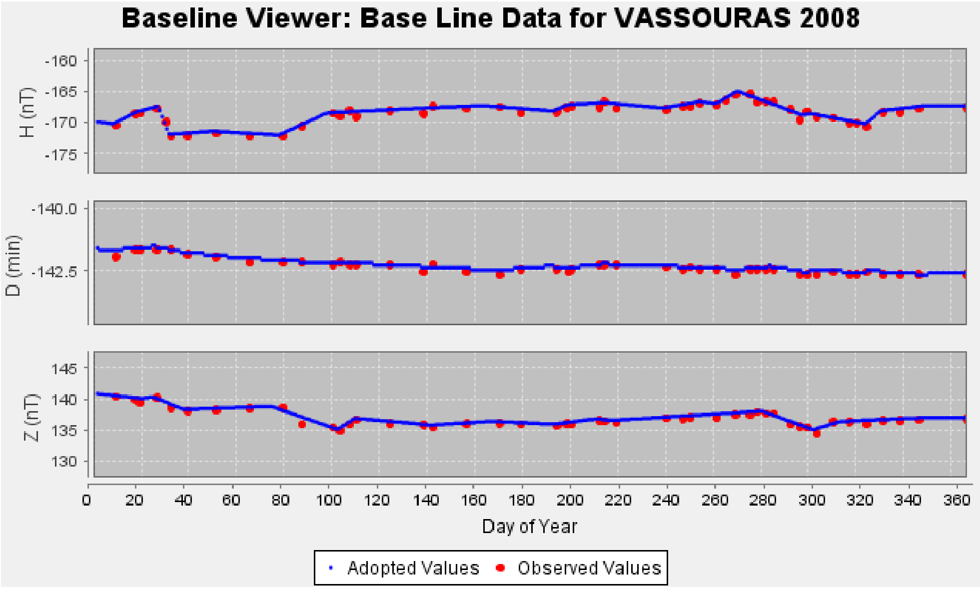

Figure 14: Baseline plots for the H, D and Z components of VSS, in 2008. No big jumps are observed, indicating the stability of the variometer. The observed values represent the absolute observations and the adopted values are interpolated using the variometer data.

Figure 15: Aerial photo of Pantanal Observatory (PNL) with its absolute hut (1), variometer hut (2), main building for energy supply control and data transmission (3) and building with guest rooms (4).

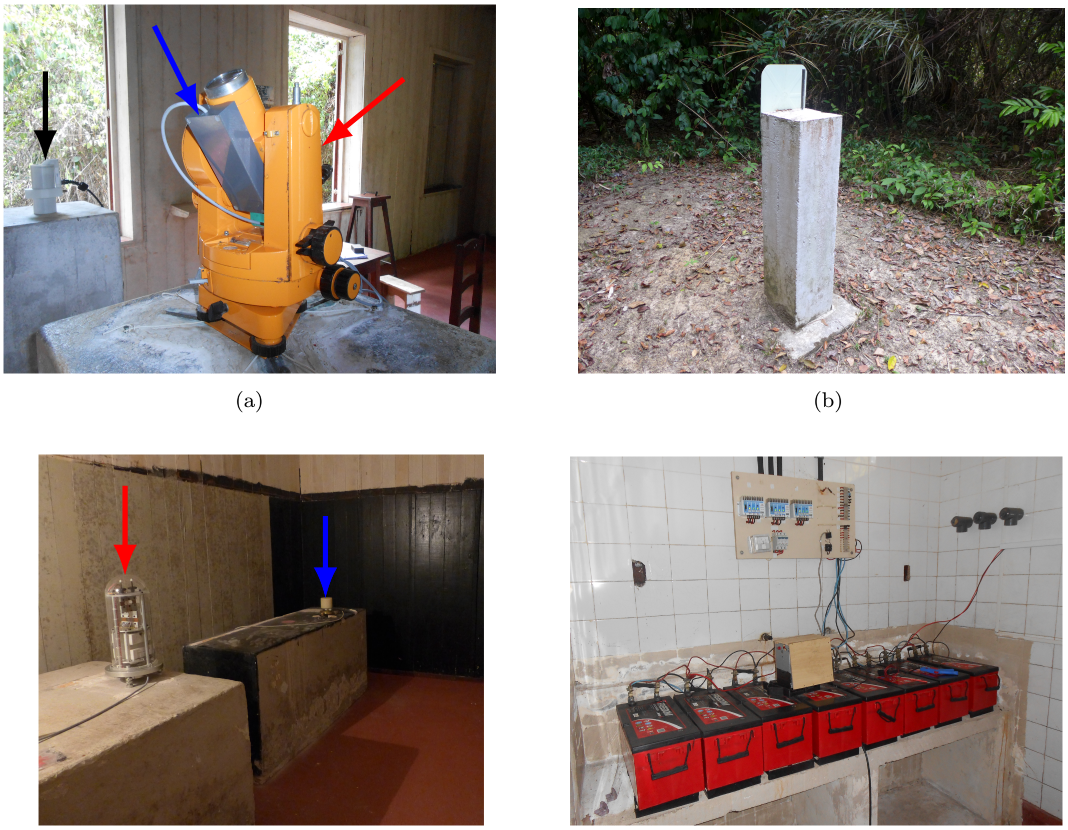

(a) (b) (c) (d)

Figure 16: Absolute equipment on their pillars, presented in (a), black arrow indicates the scalar magnetometer sensor, blue arrow indicates the fluxgate sensor and the red arrow indicates the non-magnetic theodolite. Azimuth mark (b) used during observations in Tatuoca Observatory (TTB). In (c), the red and blue arrows indicate the DTU FGE and LEMI-417 sensors inside the variometer hut of TTB, respectively. Batteries in an additional building of TTB (d), charged by solar panels, for power supply.

Only magnetic observatories can provide and guarantee a period of many decades of high accuracy data records. In addition, observatories are ideally placed at locations free of crustal anomalies or significant changes of electrical conductivity in its vicinity. On the other hand, the geomagnetic observatory network has a very irregular geographical distribution (Fig. 17), especially on the southern hemisphere and oceanic regions, which represents a limitation for global magnetic field modelling. This limitation also represents a motivation to invest in this network, in order to produce more data with high quality and more accurate global models.

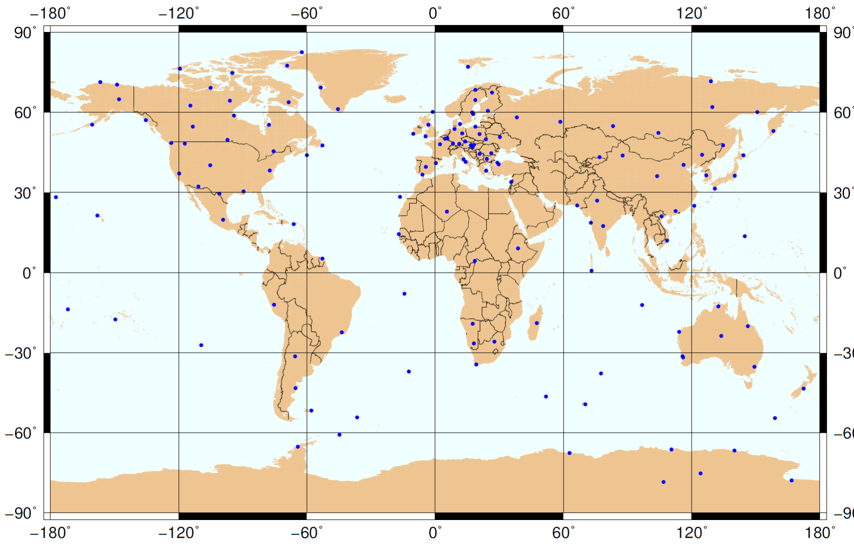

Figure 17: Map of magnetic observatories members of INTERMAGNET (blue dots).

2.1.1 Instrumentation

The magnetometers used in the procedures of magnetic observatories change with time, due to the development of new technologies. In the past, before the year 2001, all observatories used analog variometers to obtain the variation records, given in photographic paper. Similarly, the absolute instruments were quite different between the observatories.

Nowadays, the observatories started to use tri-axial fluxgate magnetometers to record the variation of the magnetic field (providing data in digital format) and one fluxgate theodolite plus a proton precession magnetometer to perform absolute measurements (Rasson et al., 2011).

The fluxgate and proton precession magnetometers are widely used in magnetic observatories, as well as in other types of magnetic surveying, and both instruments have sensitivities of 0.1 - 1 nT (Lowrie, 2007). While the fluxgate equipment measures the component of the field along its axis, the proton precession magnetometer cannot measure field components, because it is a total field scalar magnetometer.

2.2 South American Observatories

Fig. ?? shows the poor distribution of the INTERMAGNET observatories and TTB in South American, that still lacks observatory data. In this context, TTB records are very valuable both for representing a large dataset and for its special geographical position. Such peculiarities of TTB are also evident in Fig. ??, where it is possible to verify the relative position of the observatories and the magnetic equator for the years of 2008, 2012 and 2016.

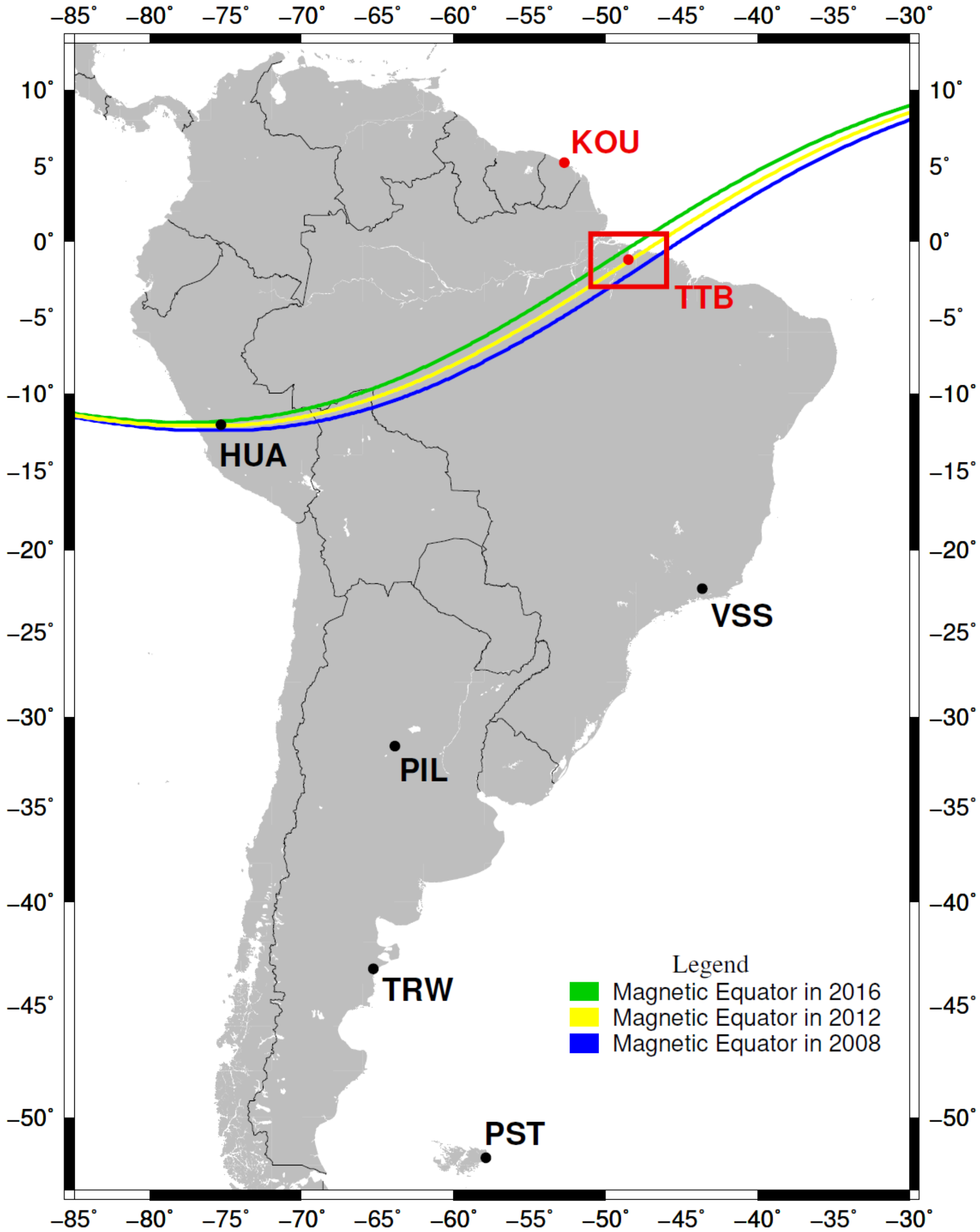

Figure 18: Geographical distribution of the South American INTERMAGNET observatories (KOU, HUA, VSS, PIL, TRW and PST), Tatuoca Observatory (TTB) and the magnetic equator for the years 2008, 2012 and 2016. Only TTB and KOU symbols are in red to distinguish the data used in this work.

TTB experienced the crossing of the magnetic equator around 2012 and, hence, it changed from the magnetic north hemisphere to the magnetic south hemisphere

(Fig. ??). Another interesting point is related to other equatorial observatory, the Huancayo Observatory (HUA, Peru), which contrasts with TTB, as its position in relation to the magnetic equator did not change significantly between the years of 2008 and 2016.

In spite of the variety of scientific subjects that can be associated with equatorial magnetic data, only a few observatories are placed at the magnetic equator. Tatuoca observatory represents one example of this scarce group, being source of accurate equatorial magnetic data. In this sense, it is convenient for data comparison and further study of the EEJ to work with a pair of stations which only one is equatorial. This is the case of the pair TTB and KOU, in which only TTB has the EEJ signal, once it is placed much closer to the magnetic equator than KOU. In addition, these stations are placed nearby the SAMA region what means that they also provide valuable data for the study of secular variation and core dynamics.

2.2.1 Tatuoca Magnetic Observatory

The Tatuoca Magnetic Observatory belongs to Observatório Nacional (ON) and it was created to measure continuously the magnetic field of the Earth. TTB was installed at the small island of Tatuoca in the Amazon River, state of Pará, Brazil, with coordinates 1.203°S 48.506°W (Fig. 19).

Despite TTB is in operation since 1957, the establishment of a permanent magnetic observatory in the north of Brazil, close to the magnetic equator, was one of the main projects of ON since as far back as 1925 (Gama, 1958). After working as a magnetic station in 1933 and several hindrances in administration and financial restrictions, the construction of a new observatory in the site happened during the 1950s (Fig. ??). More recently, in 2007, modern electronic magnetometers were installed, such as the LEMI-417M variometer (Fig. ??).

In November 2015, TTB was modernized through a cooperation between ON and The German Research Centre for Geosciences (GFZ). On this occasion, new equipment was installed: one DTU FGE variometer (Fig. ??) with a low power data acquisition system and a new DTU model G fluxgate for absolute observations. Additionally, an internet system based on the mobile phone network (Fig. ??) was installed in order to provide near real time (NRT) data transfer, aiming to attend the requirements of INTERMAGNET network.

(a)

(b)

Figure 19: Top panel (a): area in the red rectangle of Fig. ??, where Tatuoca Island is inside the yellow circle and Cotijuba Island is indicated by the number 4. Approximate distances - from Belém (1) 25 km; from Pinheiro (2) 10 km; from Mosqueiro (3) 10 km. Bottom panel (b): Tatuoca Island with an area of $63064.31\,m^2$ and its main buildings (1), variometer hut (2), absolute hut (3) and the boat of the National Observatory used for transportation(4).

(a)

(b)

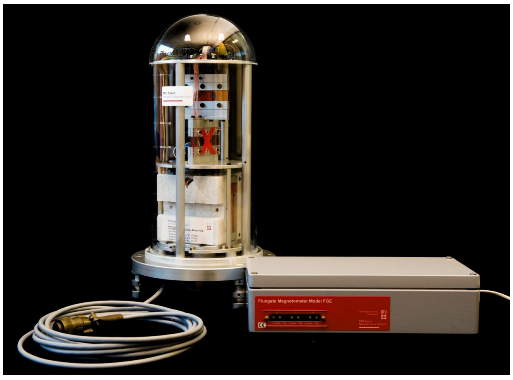

(c)

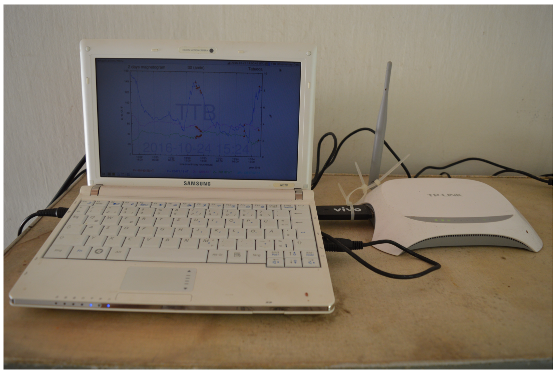

(d)

Figure 20: Top: TTB observatory structure and equipment. TTB absolute hut (a), built during the years of 1952 and 1953, photo: Jürgen Matzka. A set of a LEMI-417M variometer (b), working in TTB's variometer hut since 2007, photo taken from the user manual of the equipment. Bottom: Modernization of TTB. New FGE variometer produced by the Technical University of Denmark - DTU, recently installed in TTB (c) and laptop used to download the FGE data attached to a system with a 3G router and mobile phone network for data transmission (d).

2.2.2 Kourou Magnetic Observatory

Operated by IPGP (Institut de Physique du Globe de Paris), the Magnetic Observatory of Kourou (coastal region of French Guiana) was created in 1995 on the French Space Centre with the contribution of the Centre National d'Etudes Spatiales (Fig. 21a). The magnetic measurements in Kourou started in 1992 with a magnetic station, which became part of INTERMAGNET in 1995, with continuous observations.

KOU has the geographical coordinates 5.210°N and 52.731°W, and an elevation of 10 m. It was the first INTERMAGNET observatory in South America. The absolute instruments of KOU are one DIflux theodolite Zeiss 010A Bartington MAG01H (Fig. 21b) and one proton magnetometer GEOMETRICS G856. In the variometer hut, one homocentric fluxgate vector magnetometer works as

(a) (b)

Figure 21: Photo of Kourou Magnetic Observatory (a). Taken from http://www.intermagnet.org/imos/imos-list/imos-details-eng.php?iaga_code=KOU. Kourou absolute instrument: the theodolite and its pillar (b). Taken from http://www.bcmt.fr/kou.html.

the variometer and, for scalar measurements, one overhauser effect proton scalar magnetometer is used nowadays.

2.3 Satellite Missions

Observations of the geomagnetic field from space are made by satellite missions for more than 50 years. However, continuous satellite observations are only available since 1999. The high-precision magnetic satellite missions developed until nowadays and their corresponding key parameters, as time and altitude of operation and type of data, are listed in Table ??.

Table 1: High-precision magnetic satellite missions and their key parameters. Adapted from Olsen and Stolle (2012).

Satellite	Operation	Altitude	Data
OGO-2	Oct. 1965–Sept. 1967	410–1510 km	Scalar only
OGO-4	July 1967–Jan. 1969	410–910 km	Scalar only
OGO-6	June 1969–June 1971	400–1100 km	Scalar only
Magsat	Nov. 1979–May 1980	325–550 km	Scalar and vector
Ørsted	Feb. 1999 –	650–850 km	Scalar and vector
CHAMP	July 2000–Sept. 2010	260–450 km	Scalar and vector
SAC-C	Jan. 2001–Dec. 2004	698–705 km	Scalar only
Swarm	2013 – ...	530/<450 km	Scalar and vector

Meaning of abbreviations: CHAMP, Challenging Mini-Satellite Payload; OGO, Orbiting Geophysical Observatories; SAC-C, Satellite de Aplicaciones Cientifico-C.

The most recent mission was launched in 2013, by the European Space Agency (ESA). It is the three-satellite constellation mission Swarm (Fig. 22), which consists of a pair of side-by-side flying satellites at low altitude (450 km) and a third satellite in a higher orbit (Friis-Christensen et al., 2006).

The limitations of magnetic observatories are complemented by satellite missions, since satellites provide a true global data coverage (well distributed, with no large geographical gaps). The limitations of satellite missions are mainly due to their operation in smaller time scales and measurements in a region which is submitted to additional electrical currents and magnetic fields (not a source-free region). Observatory data is, then, used together with satellite data for field modelling. Hence it follows that the observations from magnetic observatories and

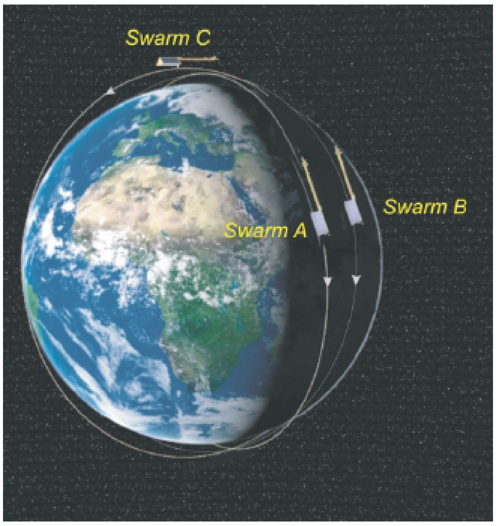

(a)

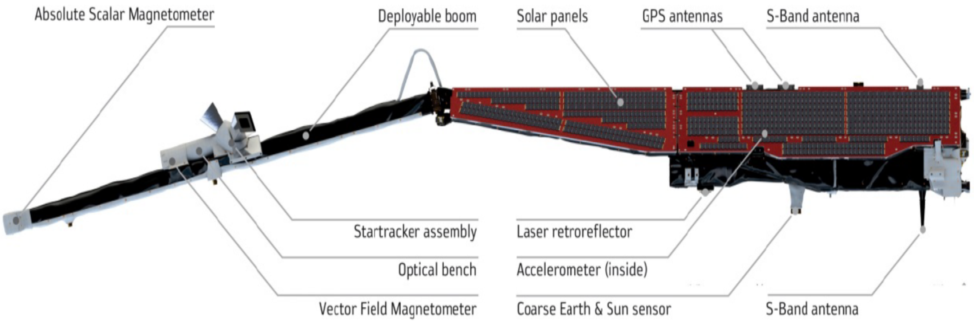

(b)

Figure 22: Scenario of the three satellite constellation that constitute the Swarm mission (a), taken from Friis-Christensen et al. (2006). Schematic location of Swarm satellites instruments (b), taken from Chulliat et al. (2015).

satellite mission complement each other, making them more valuable when combined.

3 Methodology

Data analysis is only possible once data quality is checked and calibrated. In this context, it is necessary to perform data selection, processing and preparation, which means in a chronological order the following steps: 1) the selection of a proper period of data to work with (considering the data format and acceptable noise level); 2) correction or removal of unwanted effects caused by spikes, noises, jumps and gaps; 3) perform the mathematical operations with the dataset, using a suitable computer software, aiming to produce the final result. In addition, the production of baselines are fundamental to calculate the true values of the magnetic field for a given observatory.

Therefore, this section explains how the available magnetic observatory data became ready to be interpreted. In this sense, the interpretation of data is the final step of our main motivation, which is essential to confirm expected or not expected behaviours in this dataset, to verify or emphasize the quality of TTB data and to indicate new investigations for future works. For this purpose it is convenient to work with data from nearby magnetic observatories, which makes possible the comparison between two similar datasets. To accomplish this comparison, I used the dataset of the closest magnetic observatory (Kourou) that is 852 km from TTB and outside the EEJ footprint.

This section presents: procedures of data selection, data processing and description of each technique and computational routine used for processing and statistical calculation.

The MATLAB codes used for data selection and processing were developed by Dr. Jürgen Matzka (GFZ Potsdam, Germany) and I developed codes for data preparation.

3.1 Data Selection

The selected period of magnetic data from TTB and KOU was: from June 2008 to January 2016. The available TTB raw data was obtained directly from the instruments, without any processing. Therefore, it was necessary to produce TTB final data using the variometer data and absolute observations to, lastly, compare with KOU records. KOU data was downloaded as definitive data in INTERMAGNET site (http://www.intermagnet.org/data-donnee/download-eng.php).

The choice of data period is justified by the availability of TTB data and some other practical issues as the formats of the output data files and the crossing of the magnetic equator during the chosen period. Fig. ?? shows an overview of TTB entire dataset (variometer data), presenting a timeline with information about the availability of the data. TTB is working for 60 years and it presents only one year without any variation records and some other years that need to be digitalized.

According to the computational techniques used in the data processing procedures, it would be convenient to obtain data in the specific format accepted by the programs of processing. The convenient requirements used to define the data period are listed below:

(i) TTB variation data in a digital and coherent format (see Fig. **??**). Ideally, the variation records should produce only one file per day (Table 2), containing data of all measured components (H, D and Z), with a sampling rate less or equal to one minute.

(ii) TTB absolute measurements in a digital spreadsheet (Table **??**).

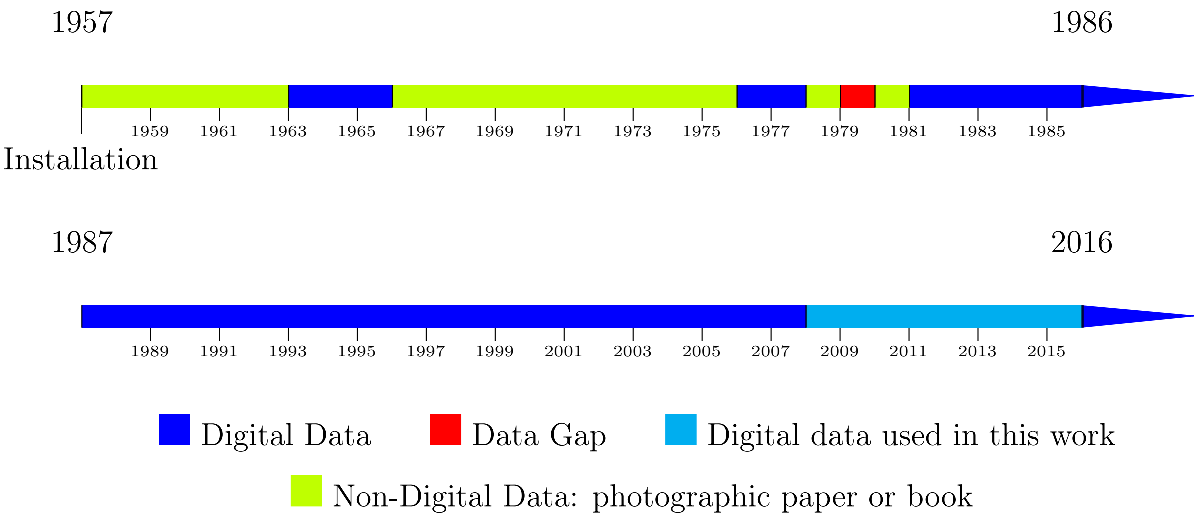

Figure 23: Timeline with the status of TTB variometer data: from 1957 until 2016. There are 59 years with data (digital and non-digital) and only 1 year without variation records.

With the information shown in Fig. **??** and Tables 2 and **??**, the selected dataset is justified, once it fulfils our presented requirements. In order to start the data calibration of recent years since the implementation of the LEMI-417M variometer and in addition to the existence of digital spreadsheets of absolute observations, the data period was easily defined as 06/2008 - 01/2016 to produce one new calibrated and useful dataset.

Table 2: TTB variometers and their data formats for different periods.

Period	Variometer in use	Output format	Available digital files
1957 - 1995	Ruska	Magnetogram*	3 files per day for H, D and Z components; hourly mean values
1996 - 2007	Ruska and digital variometers	Magnetogram* and Digital	3 files per day for H, D and Z components; hourly and minute mean values
2008 - ...	LEMI-417M	Digital	1 file per day for H, D and Z components and temperature; one second data
2015 - ...	LEMI-417M and DTU FGE	Digital	1 file per day for H, D and Z components and temperature; one second data

** Magnetograms are records in photographic paper. This type of data can be converted into digital format through appropriated software or manually.*

Table 3: Types of documentation of TTB absolute observations for different periods.

Period	Absolute Observations Documentation
1957 - 1996	Paper forms and yearbooks
1996 - ...	Paper forms, digital spreadsheets and a few yearbooks

Years without data: between 1966 - 1975 and 1978 - 1980.

The chosen data period corresponds to a number of 2792 days, from which the majority of 98% corresponds to the period of only LEMI-417M working as variometer and 2% to the period with FGE data. However, there are some data gaps in the selected LEMI records that reduced the effective quantity of days in this analysis to 2366 days. Table 4 presents the distribution of data for each variometer, sampling rates and significant data gaps.

Figure **??** indicates an interruption in the variometers records during the year of 1979, but, as expected, there are many other small data gaps related, for example, to brief power outages (caused by lightning or other natural damages to the power supply system) and not to an official interruption of the observatory instruments, as occurred during 1979. Table 4 lists some small intervals of data gaps in the case of the selected dataset.

Table 4: TTB data availability and distribution between LEMI and FGE variometers.

Year	Origin of selected data	Sampling rates*	Big data gaps (1 day or more)**
2008 (since 01/06/2008)	LEMI	0.25 s	09/12 to 31/12 (23 days)
2009	LEMI	0.25 and 1 s	27/11; 19/06 to 22/07 (35 days)
2010	LEMI	1 s	12/03 to 16/03; 02/11 to 12/11; 18/11 to 15/12 (44 days)
2011	LEMI	1 s	-
2012	LEMI	1 s	08/11 to 31/12 (54 days)
2013	LEMI	0.25, 1 and 6 s	-
2014	LEMI	1 and 6 s	02/05 to 03/06; 02/07 to 31/07; 22/08 to 28/08 (70 days)
2015	LEMI (until 19/11/2015) + FGE (since 20/11/2015)	6 s (LEMI) and 1 s (FGE)	-
2016 (until 22/01/2016)	FGE	1 s	-

** In seconds (s). ** Format of dates: DD/MM.*

Once the TTB dataset was defined, the natural sequence would be to proceed to data processing. Nevertheless, there is still one last step of data preparation: convert data to the file format used during data processing. In this sense, there is a divergence between LEMI and FGE variometers: LEMI has its output data provided as binary files, whereas FGE system provides its output already in text files (more precisely, in *.sec* files). On the other hand, the MATLAB routines used for data processing works with the *.cdf* file extension (appropriated binary format for magnetic data processing). Thus, both LEMI and FGE data needs to be converted to the *.cdf* format. However, as their original output data formats are different, they require distinct conversion processes, as schematically shown by Figures **??** and 25.

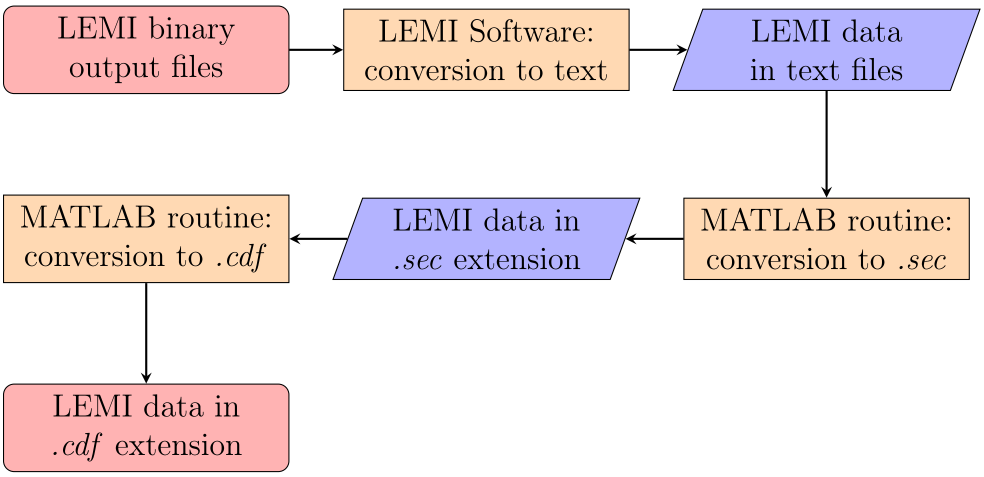

Figure 24: Flowchart indicating the necessary processes of LEMI data conversion until the final required file extension (*.cdf*) for data processing.

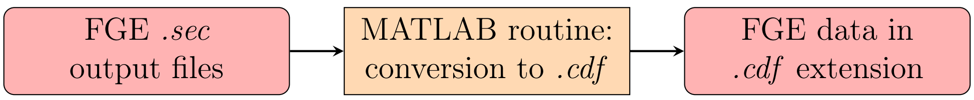

Figure 25: Flowchart indicating the necessary processes of FGE data conversion until the final required file extension (*.cdf*) for data processing.

3.2 Data Processing

It is possible to forward and process it by removing or documenting spikes, jumps and noise of the records, once data is converted to *.cdf* extension. To perform this processing of data, another MATLAB routine was used (Fig. ??). This code allows the editing of data, i.e., removal of artefacts or unwanted effects from data and then overwrite the *.cdf* file.

After verifying and processing each day of data in the considered period, the next goal was the calculation of baselines. The baseline is obtained through the variation and absolute data of TTB, with the motivation to achieve the final values of H, D and Z of an observatory. Data from variometers, in this case LEMI or FGE, provide the magnetic field components H, E (or D) and Z which may be named and defined as:

- $\mathbf{H}_{var}$ **or HN** - horizontal, approximately the north component of the magnetic field.

- $\mathbf{E}_{var}$ **or HE** - horizontal, approximately the east component of the magnetic field.

- $\mathbf{Z}_{var}$ - vertical component of the magnetic field.

Having only the variation records is not enough, as they are an approximation of the components. So, the absolute measurements are necessary to establish a reference and obtain accurate definitive values. Absolute observations from an observatory provide enough information to obtain the following magnetic field components, used in baseline calculation:

- $\mathbf{H}_{abs}$ - absolute value of the magnetic field component H.

- $\mathbf{D}_{abs}$ - absolute value of the magnetic field angle D.

- $\mathbf{Z}_{abs}$ - absolute value of the magnetic field component Z.

The expressions used to obtain H_{BL}, D_{BL} and Z_{BL}, i.e., the baselines values for H, D and Z components are calculated through the fundamental equations listed below:

$$H_{BL} = \sqrt{H_{abs}^2 - E_{var}^2} - H_{var}, \tag{2}$$

$$D_{BL} = D_{abs} - \arctan\left(\frac{E_{var}}{H_{BL} + H_{var}}\right), \tag{3}$$

$$Z_{BL} = Z_{abs} - Z_{var}. \tag{4}$$

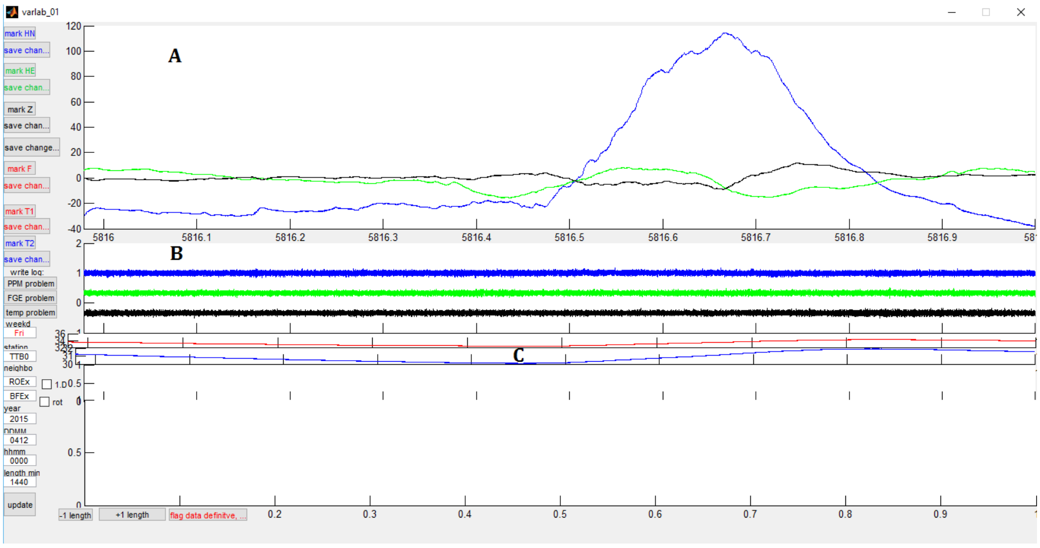

(a)

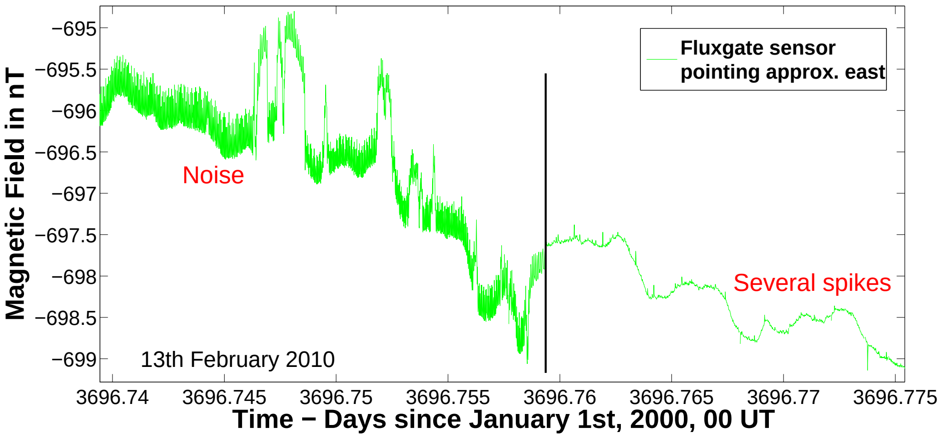

(b)

Figure 26: Function of MATLAB that uses *.cdf* files to plot data for a specific day. Top panel (a): the black letters A indicates the plot of components HN (blue), HE (green) and Z (black), B indicates the first derivative plot and C shows the temperature plot for sensor and electronics. On the left side of the panel, there are options to set the date and station (variometer) and to edit the records of the magnetic field of the selected date. Bottom panel (b): example for the HE component measured in the 13th February 2010, where a noisy signal is observed on the left of the black line and a signal with several spikes on the right of the black line.

Such calculations are made for each new available absolute measurement. But, the baseline calculation for TTB has not being done systematically for a long time. Therefore, in this work, it was necessary to accomplish these calculation for a huge amount of data without baseline. Thus, a MATLAB routine was used to calculate baselines for the entire period from 2008 until 2016 and, afterwards, another code was used to plot the baseline interpolation for each component, which were done manually, aiming the best fitting line in relation to the absolute measurements.

With the conclusion of baseline calculation and its interpolation, the production of TTB final data becomes the final goal, regarding the data processing tasks. There are four steps, all developed in MATLAB and illustrated in Fig. 27, that still remain to achieve this objective: recalculate the *.cdf* files (now considering the results of baseline determination), conversion of the new *.cdf* files into definitive files in MATLAB binary file format (MAT-files), conversion of definitive files into INTERMAGNET archive file (IAF) format and, lastly, verification of the generated IAF with the absolute observations, which are reference values.

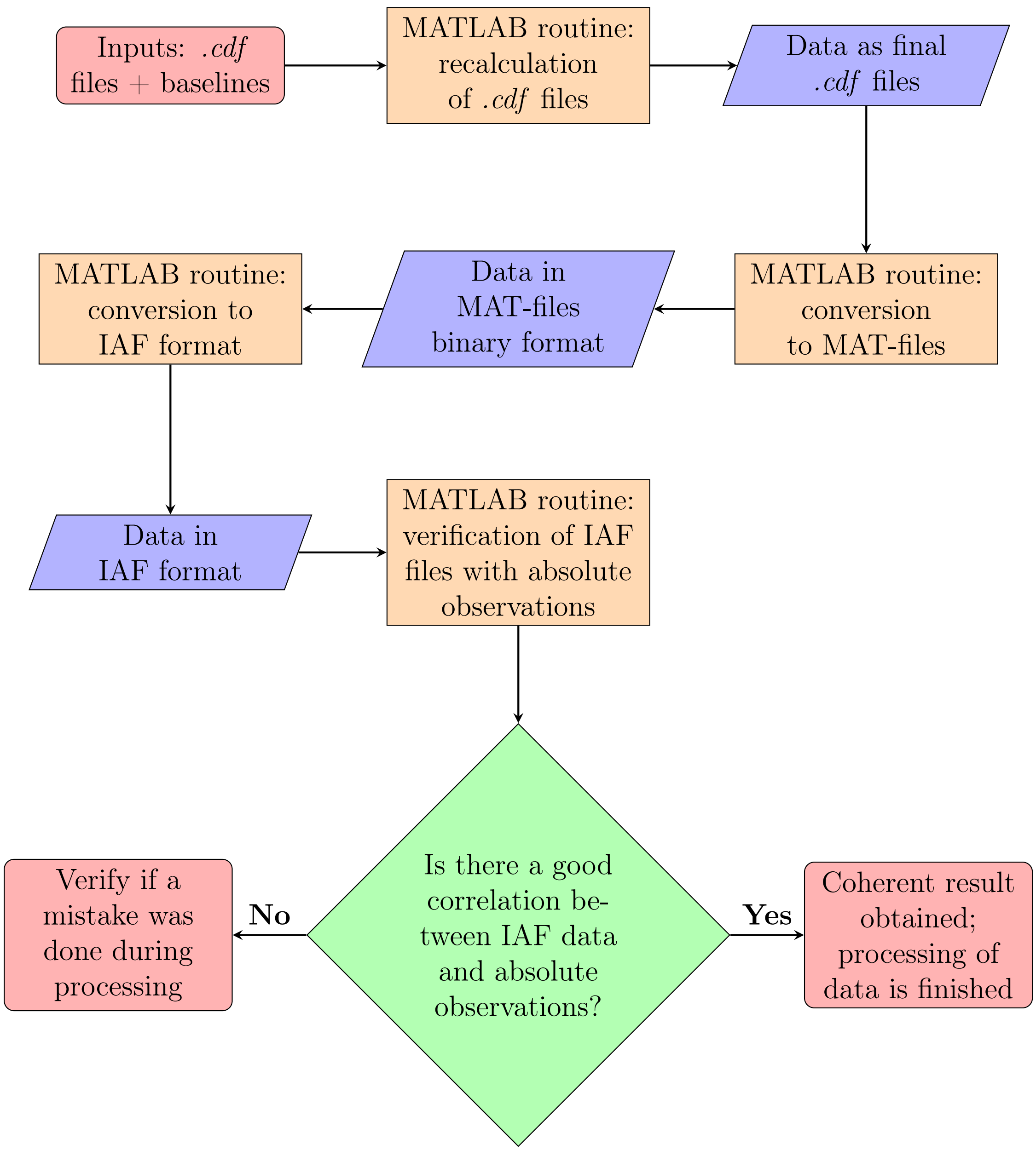

Figure 27: Flowchart illustrating the final procedures using MATLAB routines to produce TTB calibrated data.

3.3 Data Preparation

The preparation of calibrated magnetic observatories data for its interpretation depends on the interpreter's motivations and on the study being developed. In this work, the main objective presented in section 1.6 is the investigation of external field behaviour related to EEJ and CEJ in TTB, what is naturally associated to the daily variation of the H component in equatorial regions.

In this kind of analysis, it is important to have one observatory outside of EEJ area, like KOU, in order to compare two datasets with signals differing mostly in the EEJ component of the field. Otherwise the signal of the EEJ would be cancelled. Following this logic, an intuitive and practical manner to isolate the EEJ and CEJ signals recorded in TTB from the other sources of the geomagnetic field, is the result of a mathematical operation between the pair of H components from TTB and KOU, as shown below:

$$H_{DIF} = \Delta H_{TTB} - \Delta H_{KOU}. \tag{5}$$

The values of H_{DIF} are calculated for each sample point (at each minute) of the considered period of data, where ΔH_{TTB} and ΔH_{KOU} are the variation of H from the mean quiet night level of TTB and KOU records, respectively. H_{DIF} values were obtained by the subtraction, in MATLAB, of vectors loaded with TTB and KOU data. The red curve of Fig. **??** indicates the resulting values of H_{DIF} for the 5th April 2015.

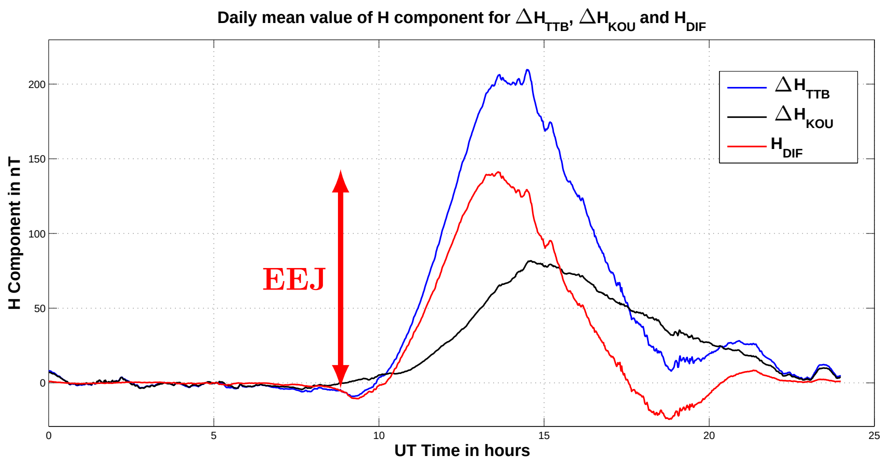

Figure 28: Plot with ΔH_{TTB} (blue), ΔH_{KOU} (black) and H_{DIF} (red) for the 5th April 2015.

It is also important to realize that the EEJ is not the only source of the daily increase in the recorded H component in both cases (TTB and KOU). ΔH_{TTB} increases during daytime due the Sq current and EEJ, while ΔH_{KOU} increases only due to the Sq current. Hence, the signal of Sq is cancelled through the calculation of H_{DIF}.

Another good reason to work with H_{DIF} is the correction of magnetic storm effects in data, as both TTB and KOU are affected by such events similarly. Therefore, it is not necessary to work only with magnetically quiet days (not disturbed by storms), keeping a significant amount of data.

The central idea of this data analysis is to use H_{DIF} values as a valuable indicator of EEJ intensity and, mainly, of CEJ occurrence. Essentially, H_{DIF} amplitude means the intensity of the EEJ effect of a given day and depressions in its curve below the night time values, either before or after the diurnal peak, indicates respectively the existence of a morning CEJ (MCEJ) or a evening CEJ (ECEJ). Fig. **??** shows clearly an EEJ amplitude of, approximately, 140 nT (indicated by the red arrow in Fig. **??**) and the occurrence of a CEJ in the beginning of the night.

With the purpose of characterizing the mentioned features of the external field in the studied region, three main analysis will be performed during data interpretation: seasonal behaviour of EEJ and CEJ, analysis of CEJ events ambiguity problem and statistics of EEJ and CEJ ocurrence, as detailed below.

3.3.1 Seasonal Behaviour of EEJ and CEJ

The seasonal behaviour of EEJ and CEJ consists of the identification of the EEJ and CEJ predominant patterns, regarding their intensity and recurrence of events, through the analysis of the average daily variation of H_{DIF}. The mean H_{DIF} values are plotted in MATLAB with respect to distinct seasonal references: during northern summer, fall, northern winter and spring. Table 5 shows which months constitute the four seasons of reference.

Table 5: Association of seasons and their months, used in this analysis.

Season	Months
Northern Winter	November, December, January and February
Spring	March and April
Northern Summer	May, June, July and August
Fall	September and October

These proposed plots represent a convenient way to set an approximated dimension of the EEJ and CEJ events for different epochs of the year in TTB. Fig. **??** shows an example of this kind of plot for the stations of ETT and HYB, in India, instead of TTB and KOU, made by Manoj et al. (2006). Thus to obtain the result for this analysis, it is necessary to define a period (the months of a season), sum the values of H_{DIF} of each day of the referred period and, then, take the mean value (average variation) for the entire period. However, the EEJ amplitude mostly depends on two main effects: a small effect (maybe negligible) from the equator position (which is dynamic, changing with time) and a large effect from the solar activity.

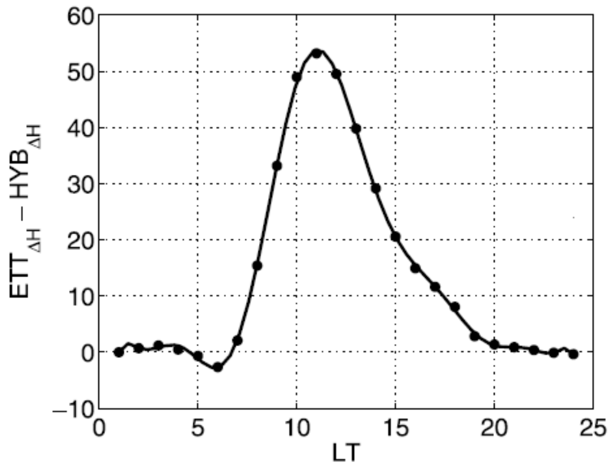

Figure 29: Example with the average difference between the horizontal component observed at ETT and HYB (ETT closer to the EEJ area), with a average strength of 53 nT of the EEJ signal, for a dataset of two years. Taken from Manoj et al. (2006).

Regarding the largest effect in the EEJ signal, from the solar activity , there is a standard process called normalization of the field component, which is applied to consider only the fluctuations around the reference solar flux level of 100, and not the total solar activity. This means that we would honor too much the solar activity influence in the EEJ amplitude if the normalization is not applied.

The EEJ amplitude will approximately scale with the square root of the F10.7 parameter[4]. Thus, the normalization process is developed following a few steps: recalculation of the H_{DIF} plots for solar flux level of 100 by dividing the H_{DIF} values by the square root of the annual mean of the F10.7 parameter of the respective year and the subsequent multiplication with the square root of 100, as the expression below:

$$|H_{DIF}| = \frac{H_{DIF}}{\sqrt{\phi}} \times (\sqrt{100}), \tag{6}$$

where $|H_{DIF}|$ means the normalized H_{DIF} and ϕ is the solar flux annual mean.

3.3.2 Analysis of CEJ Events Ambiguity Problem

Although the identification of a CEJ event by using the H_{DIF} plot is very intuitive, the interpreter needs to be sure of such an event before starting the statistics,

[4]The F10.7 parameter, also called solar flux, describes the solar activity for a given year and month. It was obtained in the file: ftp://ftp.geolab.nrcan.gc.ca/data/solar_flux/monthly_averages/solflux_monthly_average.txt

with the purpose of avoiding misinterpretation and inconsistencies in the developed analysis.

The detection of CEJ events must be done very carefully, because negative peaks in the H_{DIF} plot could be produced by a summer/winter effect concerning the sunrise and sunset times in stations at different latitudes. To illustrate this effect, let us consider the example presented in the box below:

Consider a station AAA at the magnetic equator and a station BBB at the same longitude, but at a higher northerly latitude. Then, there would be two situations:

1. Around June, the sun would rise earlier and set later at station BBB.

2. Around December, the sun would rise earlier and set later at station AAA.

The situations shown in the box could be applied, with some approximation, to the pair of stations TTB-KOU, in which TTB would represent the station AAA and KOU, the station BBB. In addition, the order of the sunrise and sunset between the stations can compensate their difference in longitude and, then, produce negative values of H_{DIF}, due to the relation of the sun and the ionospheric currents. Hence, it is necessary to study this summer/winter effect, in order to verify if this compensation of TTB and KOU longitudes occurs. If this happens, depressions in H_{DIF} plots could be observed and interpreted, mistakenly, as a CEJ.

To avoid this type of mistake, the order of the sunrise and sunset times at a height of 108 km above sea level (ionospheric region of the EEJ) were defined accurately for TTB and KOU, using one implemented MATLAB routine based on an astronomical algorithm stated by Meeus (1998) and, then, they were plotted versus the day of the year, what allows the detection of potential situations of erroneous interpretation of CEJ events.

3.3.3 Statistics of EEJ and CEJ Ocurrence

Statistical analysis of the occurrence and distribution of the EEJ and CEJs[5] for the period of data, motivated by the possibility to investigate about the correlation between the EEJ/CEJ occurrence and the moment of its occurrence, during the days and years, were performed. In order to understand better the conditions for the EEJ/CEJ events and their relation with the sun, another MATLAB routine was written to automatically detect EEJ/CEJ events and produce statistical information, as their distribution and intensity during the seasons, based on the manipulation of the generated H_{DIF} vectors of data.

The MATLAB routine gathers the EEJ intensities by saving the maximum H_{DIF} value during daytime. The code does the opposite to detect CEJ events: it takes the minimum value before and after the positive peak. After these detection procedures, the program saves the values in 12 vectors, which correspond to the months of the year, so it is guaranteed that the saved information is separated per months. With the monthly separation it is also possible to calculate the mean values, which do not consider data gaps in the calculation, and percentages.

However there is a slight difference between the detection of the occurrence of EEJ and CEJs: the EEJ effect is already given by the H_{DIF} increase during daytime as explained in this section, but, on the other hand, the CEJs are not determined so obviously. It is necessary to establish a reference condition to consider a depression in H_{DIF} as a CEJ, because not all negative peaks represent a CEJ. This reference will be called as the threshold value.

The chosen threshold value in this case was -10nT. So, any value right before or after the daily positive peak of H_{DIF}, which is lower than -10nT was considered a CEJ event. This concept is extremely convenient, once it can be easily applied as filter using a MATLAB code, in order to detect and quantify the occurrence of this phenomena. Using this condition, the standard statistical procedures are possible to be done with the CEJ events information.

[5] CEJs means more than one CEJ.

4 Results

The results for each procedure of data analysis are presented in this section and they are divided in four topics: 1) data processing and baseline plots, 2) seasonal average behaviour of H_{DIF}, 3) the ambiguity problem of CEJ events and 4) the statistics done using the obtained EEJ and CEJ information.

4.1 Processing Results and Baseline Plots

Some important results obtained during data processing are reported in order to define some crucial aspects of data quality. Data processing documentation indicated some significant recurrent noises in LEMI data and four jumps in this dataset were observed, which are usually associated to sensor rotation in the variometer hut. Table ?? shows the distribution of the documented artificial disturbances and jumps for the time length in analysis. Fig. 30 presents a typical example of a day with significant noise level during daytime as reported in Table ??.

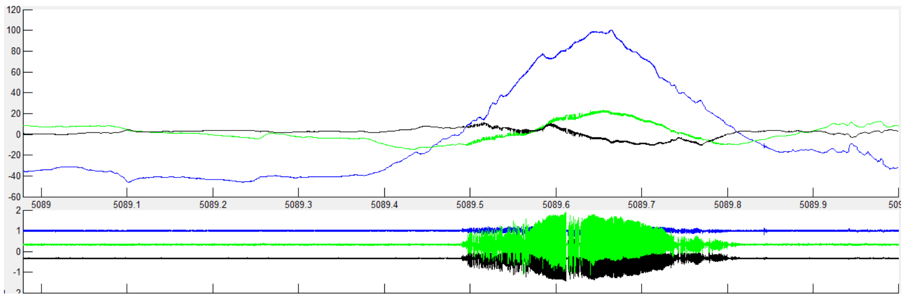

Figure 30: Strong disturbance of 2 nT during daytime of 07th December 2013 in TTB. The first derivative plot (bottom) indicates the presence and magnitude of noises, which is in this case, intense in HE and Z components (green and black), but almost zero in the HN component (blue).

These referred daily noises can be possibly credited to an electronic interference. A potential source of noise in this case can be the solar panel system of TTB, what justifies the high noise level only during daytime.

Another important result obtained from data processing are the baseline plots, which are useful to verify the quality of data and its stability. Baseline information may be used together with the processing documentation to provide a very detailed description of the available dataset. The referred plots are given in Figures 31, ?? and 33.

Table 6: Distribution of recurrent noises and occurrence of jumps (sensor rotation) in TTB data along the time.

Year	Intensity of Recurrent Noises	Noise Time Occurrence	Sensor Rotation Occasions*
2008	0.5 nT mostly in E and Z	Daytime	-
2009	0.5 to 4.5 nT mostly in E and Z	Daytime	29/08
2010	0.5 to 4.5 nT mostly in E and Z	Daytime	24/11
2011	0.5 to 2.5 nT mostly in E and Z	Daytime	-
2012	0.5 to 1.5 nT mostly in E and Z	Daytime	-
2013	0.5 to 5 nT mostly in E and Z	Daytime	07/11
2014	4 to 5 nT mostly in E and Z	Daytime	-
2015	-	-	13/11
2016	-	-	-

** Format of dates: DD/MM.*

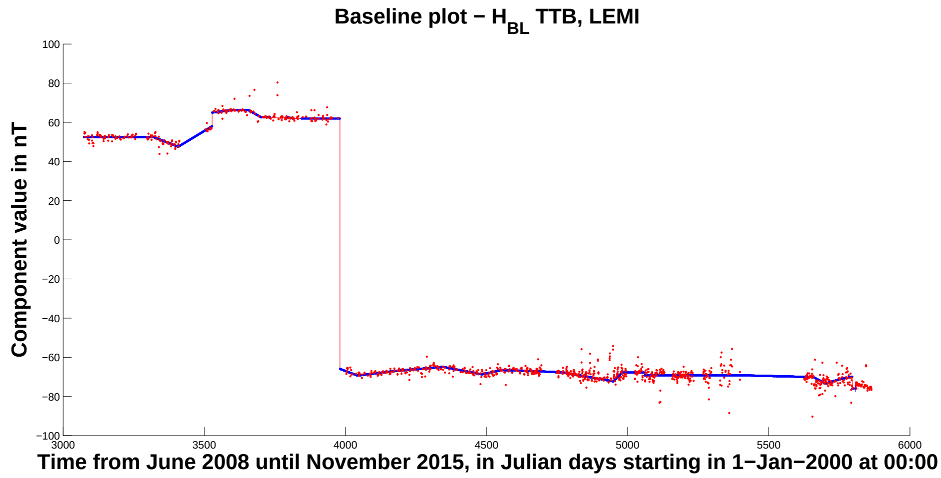

Figure 31: Baseline plot for TTB H component for LEMI variometer. Red dots: absolute observations. Blue line: interpolated baseline.

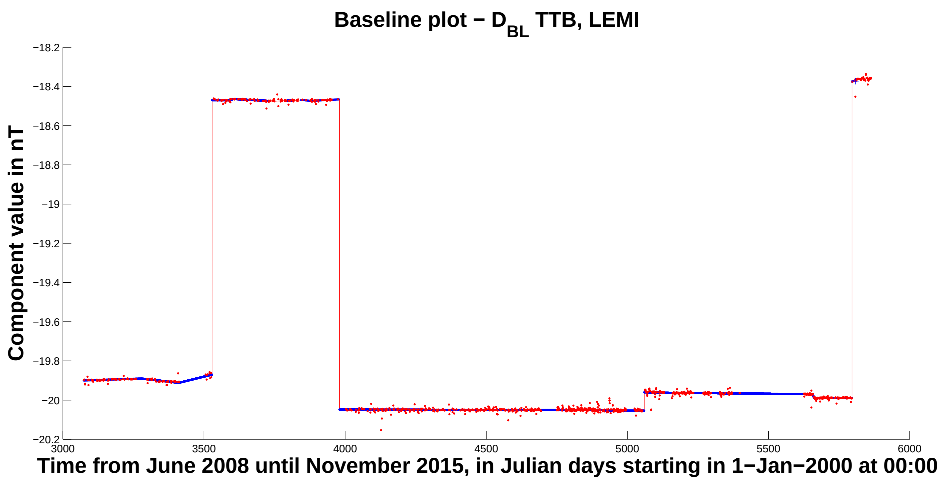

Figure 32: Baseline plot for TTB D angle for LEMI variometer. Red dots: absolute observations. Blue line: interpolated baseline.

It is clear that all three baselines are not stable during the entire period. There are four main events of jumps in the baseline plots. These jumps are easily justified as a consequence of the four sensor rotations observed during data processing and its documentation, as shown in Table **??**. Such sensor rotations may have been caused by a necessary maintenance inside the variometer hut or, maybe, because the technical staff were not properly informed about the prejudices of moving the sensors. Nevertheless, in a general perspective, TTB baselines can be considered

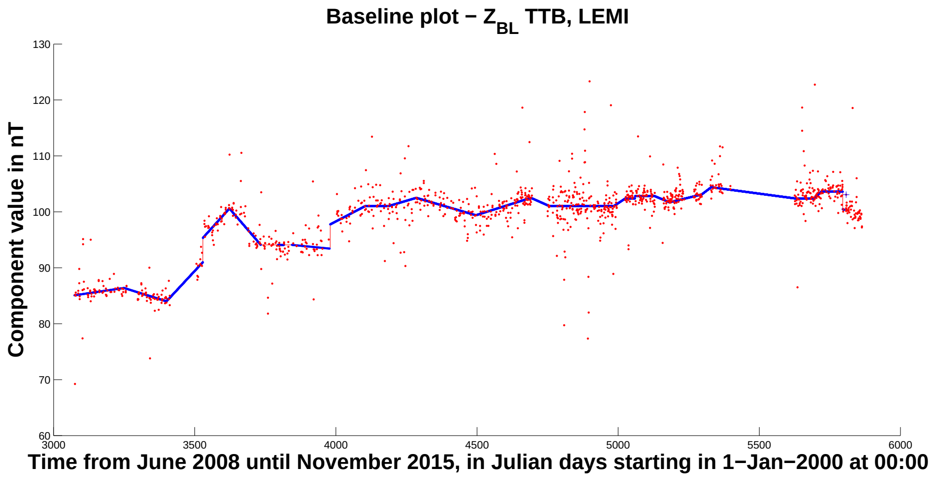

Figure 33: Baseline plot for TTB Z component for LEMI variometer. Red dots: absolute observations. Blue line: interpolated baseline.

as satisfactory.

The observed jumps in LEMI baselines are not the same in all components. This is expected, because it depends on how the sensor was moved or rotated. The vertical component is not affected likewise the horizontal component and declination, because the sensor is moved horizontally along a levelled surface.

The remaining baseline plots for the period between November 2015 and January 2016 (2% of the dataset) correspond to the period with FGE recording data as well. They are demonstrated in Figures **??**, 35 and **??** for H, D and Z components respectively.

The first results of FGE baselines present a very stable trend. There is a small jump in the beginning of the FGE baselines, but it is probably associated to the implementation of the instrument. It is also clear that the baselines for FGE H and Z components fit better to the absolute measurements than the declination baseline. This variation in declination absolute measurements shown in Fig. 35 may be explained by the natural variations from one observer to another when performing the absolute measurements procedures.

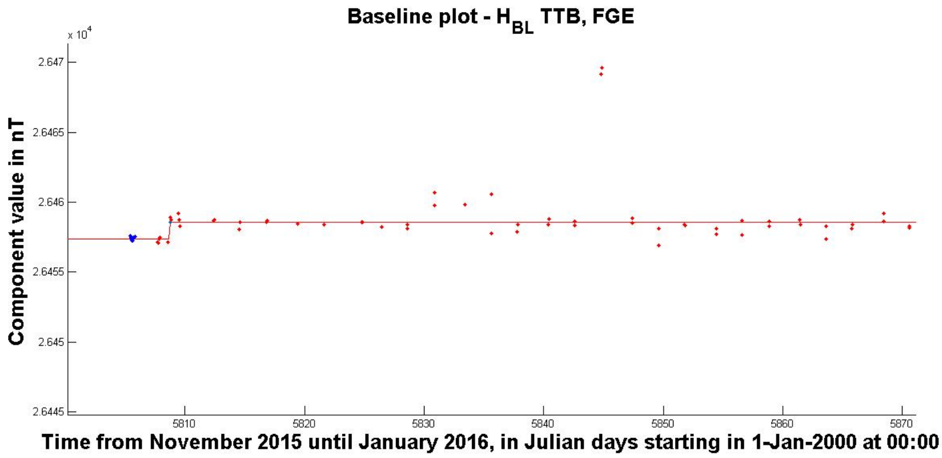

Figure 34: Baseline plot for TTB H component for FGE variometer.

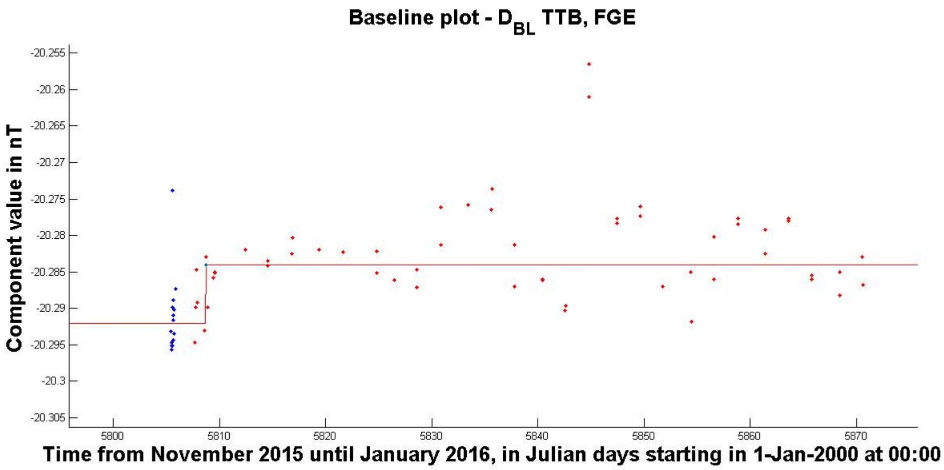

Figure 35: Baseline plot for TTB D angle for FGE variometer. Red dots: absolute observations. Blue line: interpolated baseline.

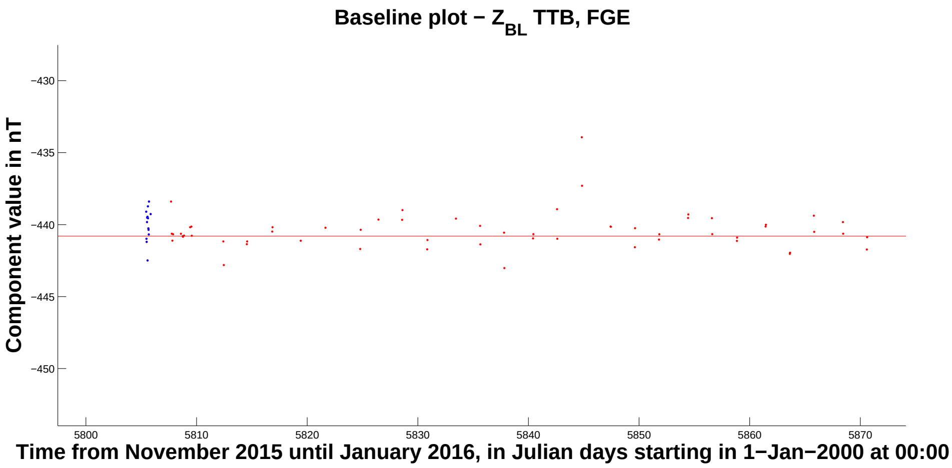

Figure 36: Baseline plot for TTB Z component for FGE variometer. Red dots: absolute observations. Blue line: interpolated baseline.

4.2 Seasonal Average Behaviour of H_{DIF}

Figures 37, ??, 39 and ?? show the obtained plots for the average daily variation (or mean H_{DIF} values) normalized to the F10.7 parameter for the northern winter, spring, northern summer and fall periods between 2008-2015, respectively. One peculiarity of these plots are the presence of four curves for each season. All these curves represent the normalized H_{DIF} values, but for distinct epochs: 2009-2010 (red), 2010-2012 (blue), 2012-2014 (green) and 2014-2015 (black).

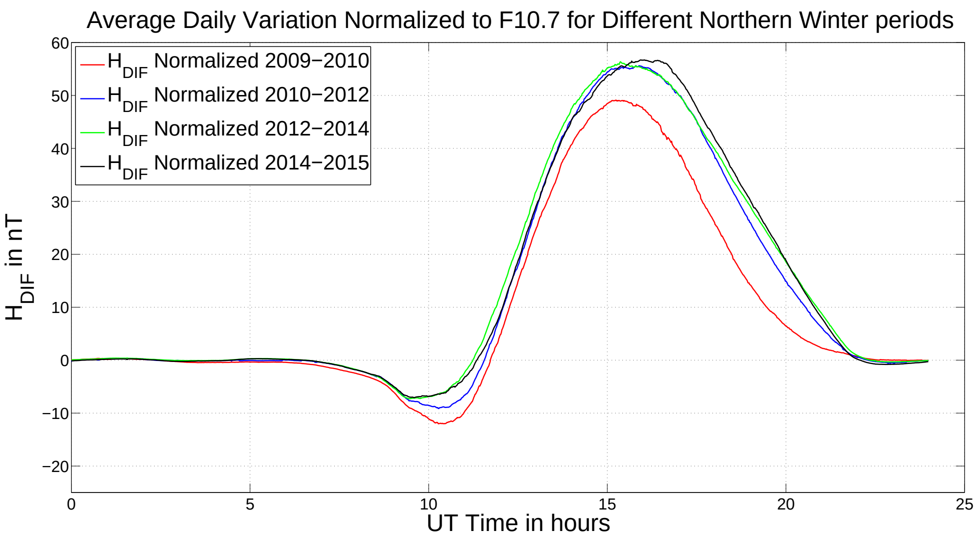

Figure 37: Normalized average H_{DIF} for the northern winter periods between 2008-2015.

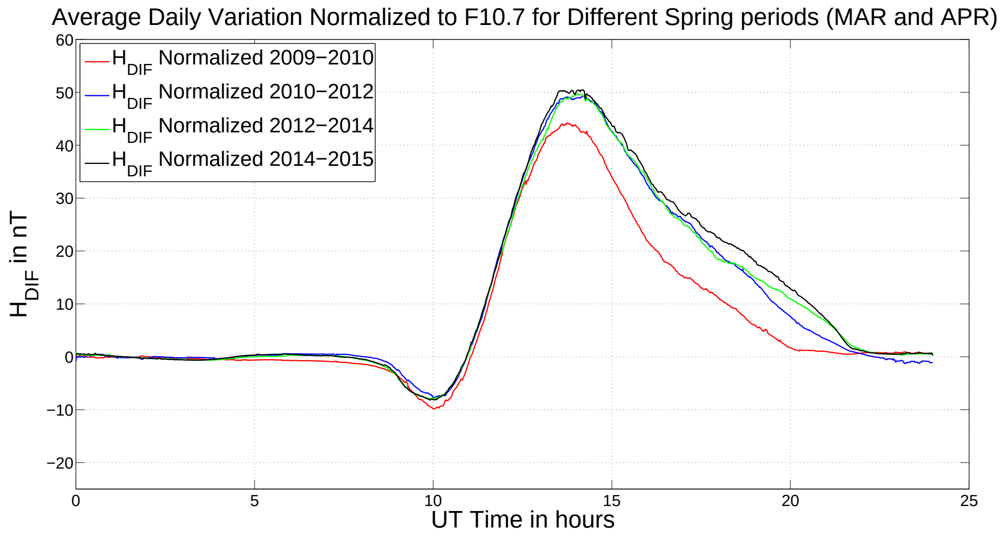

Figure 38: Normalized average H_{DIF} for the spring periods between 2008-2015.

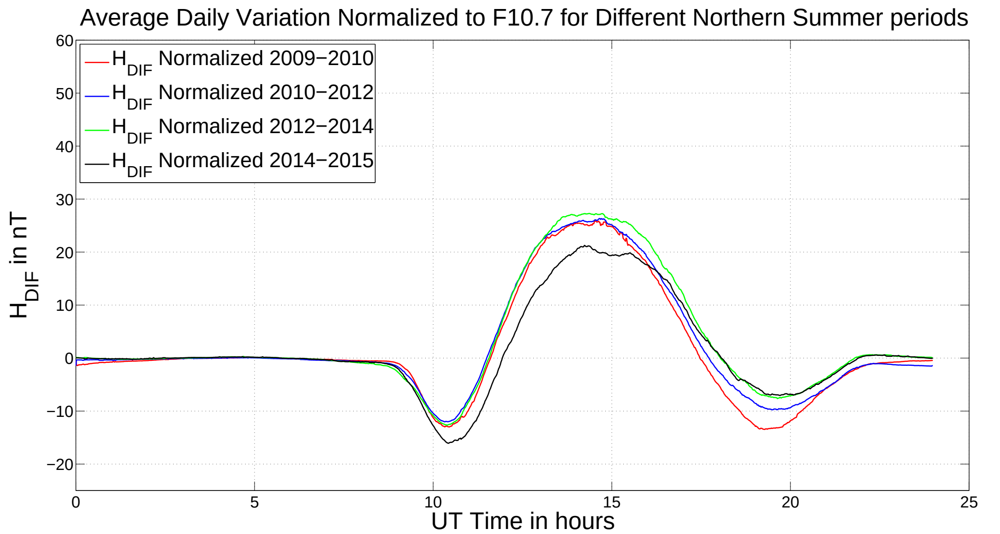

Figure 39: Normalized average H_{DIF} for the northern summer periods between 2008-2015.

The differentiation of the normalized H_{DIF} in four epochs allows the identification of the effects of the relative position of TTB with respect to the dynamic magnetic equator, which is one of the two main agents that controls the EEJ amplitude (as detailed in section 3.3.1). That is why the red (2009-2010) and black (2014-2015) curves present, often, the largest differences of behaviour, as they represent, in a chronological order, the beginning and the end of the dataset. This relation is also clear in Fig. **??**, where the positions of TTB and the magnetic equator for three different moments (2008, 2012 and 2016) is illustrated.

An interesting point concerning the plots for northern summer is: the highest

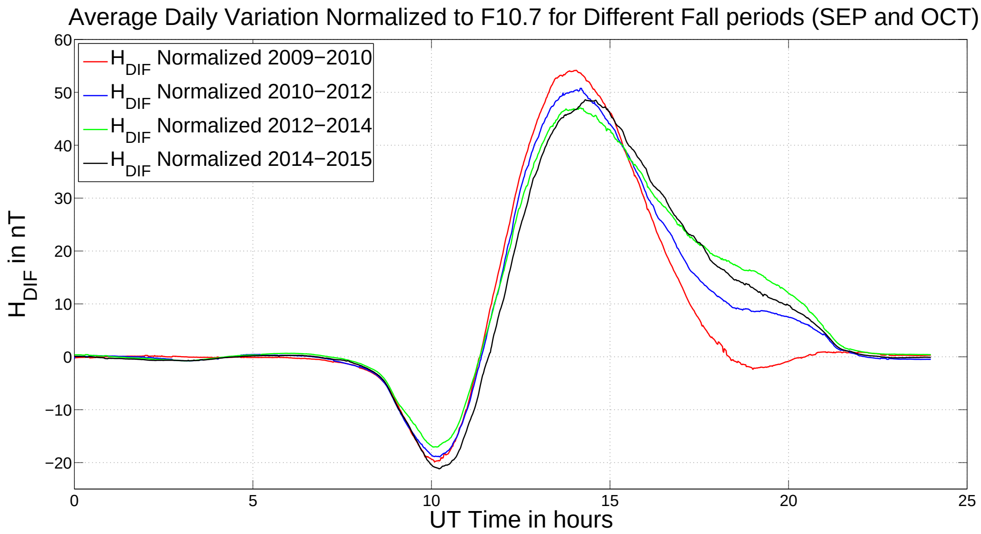

Figure 40: Normalized average H_{DIF} for the fall periods between 2008-2015.

values of H_{DIF} were observed for the periods 2010-2012 and 2012-2014, which are related to the epoch of the magnetic equator crossing in TTB. Intuitively, it could be expected to find this result for all seasons, but this behaviour was only observed for northern summer, as it represents the minimum influence of the solar flux in the EEJ amplitude.

Another clear result observed from the plots of the normalized average H_{DIF} is the variation of the EEJ amplitude and potential CEJ events during the four seasons. The northern winter (November, December, January and February) curves present the highest values of EEJ amplitude (around 55nT) and the northern summer (May, June, July and August) is the opposite, with values around 25nT. The maximum values for the equinoxes are restricted between the northern winter and northern summer peak values.

It is also possible to get some information about the occurrence of CEJ events and their intensity, as the typical depressions before or after the positive peak are observed in all cases, with a higher mean intensity for northern summer and fall periods.

4.3 Ambiguity Problem of CEJ Events

The MATLAB routine used to calculate accurately the sunrise and sunset times for TTB and KOU produced, as output, the following results for the ionospheric height of 108km:

1. The sun always rises earlier in TTB ionosphere than KOU ionosphere.
2. The sun always sets earlier in TTB ionosphere than KOU ionosphere.

This result is better observed graphically, through Fig. 41, which only the times for the year of 2015 are plotted (it does not make sense to plot more than one year in this case), focusing in the ionospheric level.

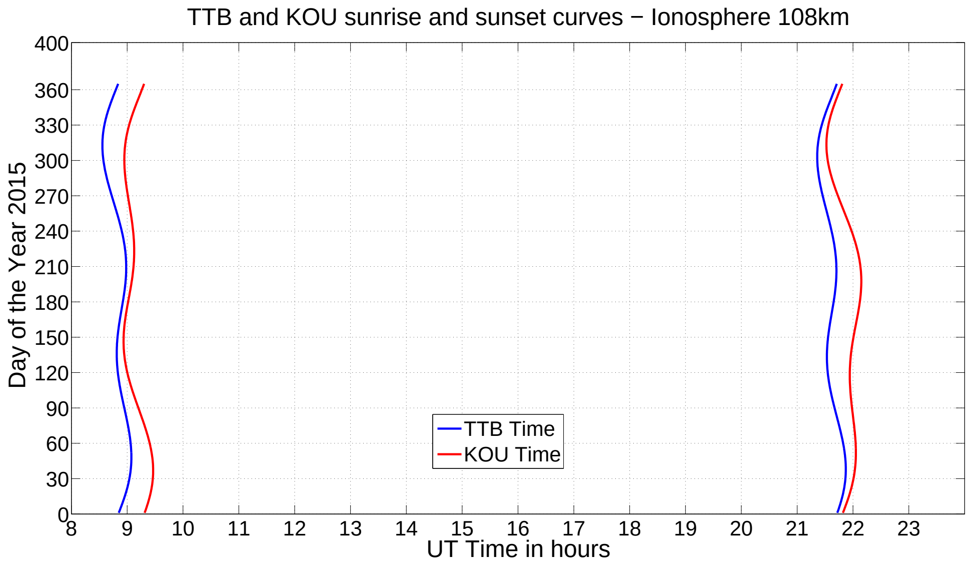

Figure 41: Curves for the sunrise times of TTB and KOU (around 9UT) and sunset times (between 21UT and 22UT) for the year of 2015.

As KOU lies more to the west than TTB, the sunrise and sunset are generally later in KOU, as seen in Fig. 41. In December, the sun is more distant from KOU, so it has a short day and long night. It means that its sunset time will be more similar to TTB around day 0 and 365 than in July (day 180). In July, the sun is closer to KOU than TTB, so KOU has longer days and its sunrise starts earlier, what means that, in July their sunrise times are more similar. It is even easier to check the difference between TTB and KOU times, by the plots in Figures **??** and 43.

Although the sunrise and sunset always happen first in TTB, there is, still, a significant distinction between the epochs of summer and winter. Both plots of Figures **??** and 43 describe this difference between the solstices. TTB sunrise happens almost 30 minutes earlier than KOU in December and this difference is almost 5 minutes in July (Fig. **??**). On the other hand, the relation for sunset keeps the same relation, but in this case the 30 minutes difference happens close to June and around 5 minutes for December (Fig. 43).

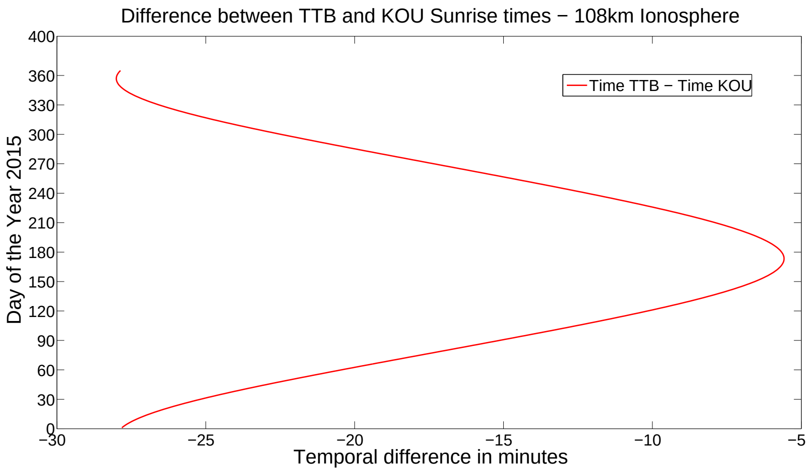

Figure 42: Curve for the difference between TTB and KOU sunrise times at the ionosphere. The time values were kept negative, as they indicate that TTB sunrise occurs first.

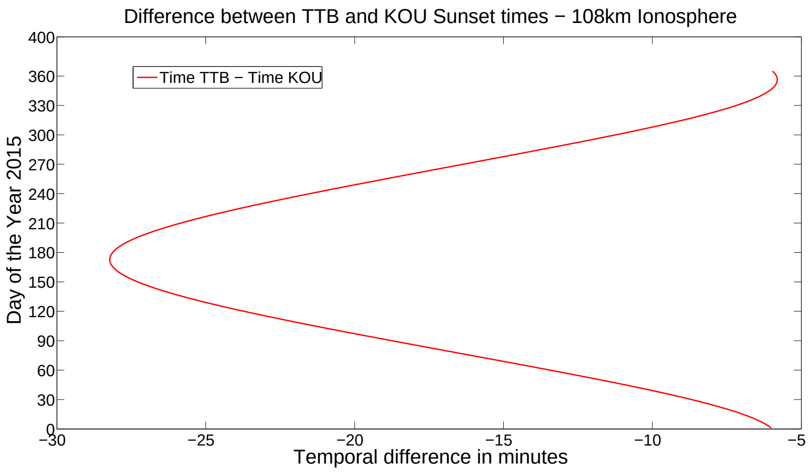

Figure 43: Curve for the difference between TTB and KOU sunset times at the ionosphere. The time values were kept negative, as they indicate that TTB sunset occurs first.

4.4 Statistical Analysis of EEJ and CEJ Occurrence

The statistical analysis of EEJ intensity and the frequency of occurrence of CEJ events are reported in this section. Note that the entire dataset was used to produce all the statistical information. Data gaps were automatically excluded by the MATLAB code used to produce the statistical information.

In Fig. **??**, the distribution, per month, of the average EEJ intensity is given. It is evident how the EEJ amplitude depends on the season of the year, as its strength is strongest in December/January and weakest in June/July, because the electronic density in the ionosphere varies along the year and, hence, affects the

EEJ intensity.

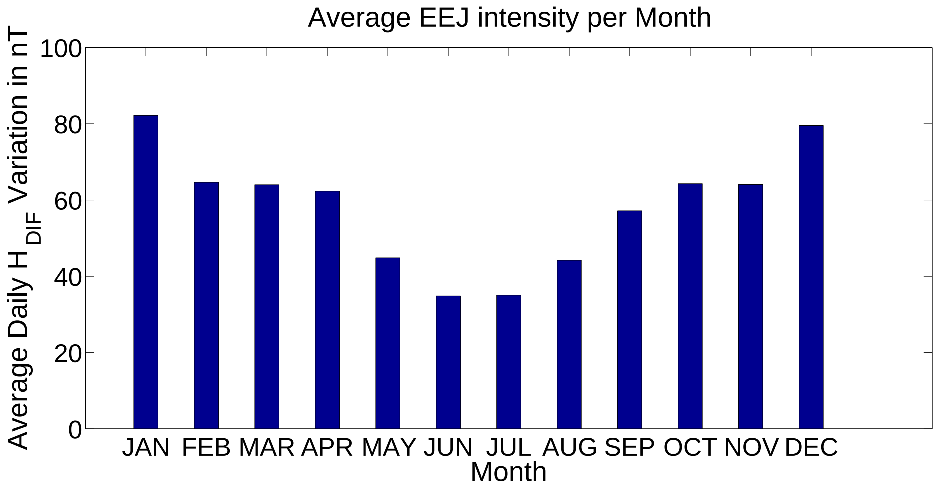

Figure 44: Distribution of the EEJ average intensity per month using the entire dataset.

Concerning the CEJ occurrence, Table 7 presents a general overview, which lists the quantity and percentages of MCEJ and ECEJ in relation to the total number of days of the dataset without gaps (2366 days) and the ratios between them. Due to the specific equatorial ionospheric conditions in the region of TTB, the MCEJ events (69.4%) are much more frequent than ECEJ (36.0%).

Table 7: Occurrences of morning and evening counter-electrojets (MCEJ and ECEJ) in Tatuoca, for the period 2008-2016.

Station	**MCEJ** Quantity (percent.)	**ECEJ** Quantity (percent.)	**Ratio** (MCEJ/ECEJ)	**Ratio** (ECEJ/MCEJ)
Tatuoca	1641 (69.4%)	852 (36.0%)	1.9	0.5

The distribution of CEJ occurrence per month was divided in two types of analysis: frequency of MCEJs (Fig. **??**) and frequency of ECEJs (Fig. 46). The two patterns of distribution obtained are not similar: while Fig. **??** shows the high values of MCEJ frequency (more than 40% for all months) and peak values during the fall, Fig. 46 indicates the concentration of ECEJs around a peak value in July (with only 5 months with more than 40% of frequency). The CEJ events are usually observed with more frequency during the months with minimum solar activity (Almeida, 2011) and this is in agreement with the result found for ECEJ, but not for MCEJ result.

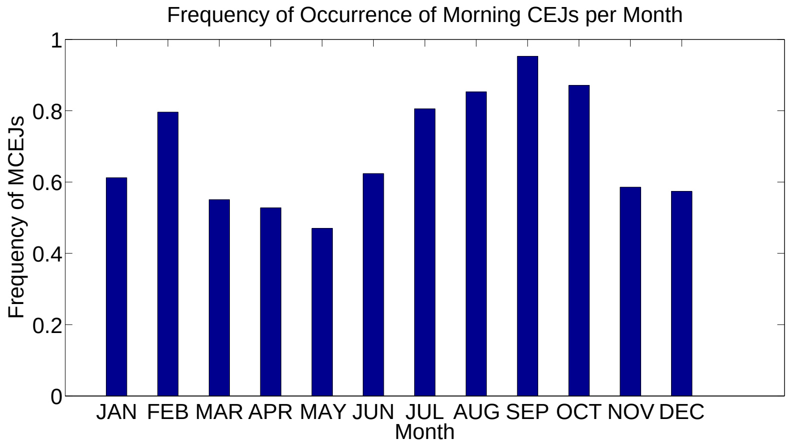

Figure 45: Frequency of occurrence of MCEJs per month (where $1 = 100\%$), using the entire dataset.

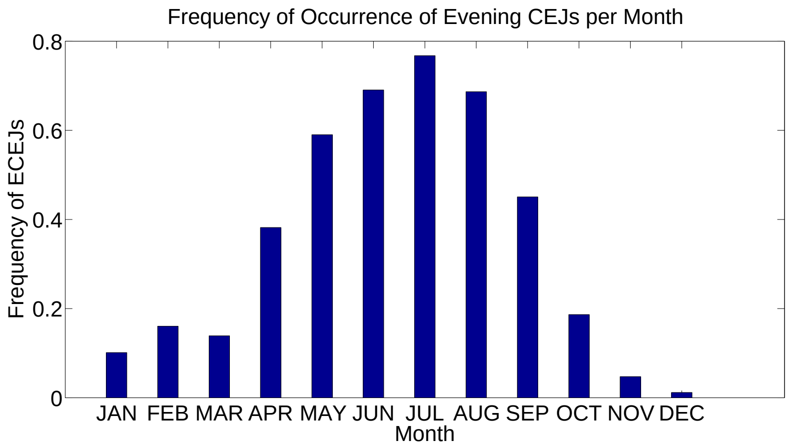

Figure 46: Frequency of occurrence of ECEJs per month (where $1 = 100\%$), using the entire dataset.

5 Conclusions

Tatuoca Observatory represents a reliable source of data for main field and especially for equatorial external field studies. The calibration and interpretation of such a long dataset (seven years and a half) of TTB modern variometers constitutes an expressive result in the Brazilian and international perspectives, especially for the research concerning the ionospheric effects of EEJ and CEJ, due to the position of TTB at the magnetic equator.

Concerning the data processing, it is evident that some recurrent artificial disturbances affected the data, which are probably associated to the solar panel system. Fortunately, these noises were extinguished with the installation of the FGE variometer and with some improvements in TTB power supply system, during its modernization. Although the observed noises do not invalidate our analysis, because their intensity were not higher than 5 nT, it is necessary to improve the quality control of TTB data, in order to avoid noises and obtain the final product as best as possible.

The LEMI baselines presented some occasions of sensor rotation, which effects were posteriorly corrected, while the FGE initial baselines seems to be very stable. As in the case of recurrent noises, the quality control must extinguish the baseline jumps. This could be easily done by means of training and courses developed to the TTB technical staff.

It was, then, observed that the EEJ signal changes with respect to a long time scale, in which the position of the station in relation to the magnetic equator changes gradually with time and controls part of the EEJ amplitude, and it also varies with respect to a shorter time scale, related to the seasons of the year and, hence, to the seasonal variation of the solar flux, controlling most of the EEJ intensity. It was also indicated that the northern summer season may be the best period to observe the control of the magnetic equator proximity in the EEJ signal, as the solar flux is minimum during this epoch.

The analysis of CEJ events distribution is intrinsically connected to the verification of the origin of negative H_{DIF} values. Although some significant differences between the sunrise and sunset times for TTB and KOU were detected, the time interval of such differences ranges only from 5 to 30 minutes. This fact probably excludes any possibility of misinterpretation of CEJ events (as commented in section 3.3.2), as the maximum time difference is close to 30 minutes. This time is, still, a short time when compared to the duration of CEJ events that causes the negative H_{DIF} values, lasting about 1 or 2 hours. Thus, the statistical study about CEJ occurrence can be considered as valid and it revealed that the monthly distributions of morning and evening CEJ events are different and the MCEJs are more frequent. The obtained result may indicate that the ECEJs depend more on the solar flux intensity than the MCEJs and this higher dependence of the ECEJs also justify its smaller percentage of occurrence.

5.1 Future Work

The results found for the distribution of MCEJ and ECEJ events would require a more detailed analysis, which I would do considering the dynamics of the ionosphere and all parameters that control the EEJ, to conclude the process of interpretation.

Another goal for the near future is to work with the remaining TTB data in digital format and digitalize the old records still in photographic paper.

Meanwhile, all efforts will be concentrated to set TTB as an INTERMAGNET observatory, controlling its data quality to prevent the records from noises and other undesired effects.

6 Bibliography

Almeida, P. D. S. C., 2011. Relação entre a ocorrência do contra eletrojato equatorial e o aparecimento de oscilações de pequena escala na regiãoo e. Master's thesis, INPE.

Amit, H., 2014. Can downwelling at the top of the Earth's core be detected in the geomagnetic secular variation? Physics of the Earth and Planetary Interiors 229, 110–121.

Baumjohann, W., Blanc, M., Fedorov, A., Glassmeier, K.-H., 2010. Current Systems in Planetary Magnetospheres and Ionospheres. Space Sci Rev 152, 99–134.

Baumjohann, W., Nakamura, R., 2007. Treatise on Geophysics, Chapter 5.03, Magnetospheric Contributions to the Terrestrial Magnetic Field. Vol. 5. Elsevier.

Beggan, C., Macmillan, S., Clarke, E., Hamilton, B., 2014. Improving models of the Earth's magnetic field for directional drilling applications. First Break 32, 53–60.

Beggan, C. D., Beamish, D., Richards, A., Kelly, G. S., Thomson, A. W. P., 2013. Prediction of extreme geomagnetically induced currents in the UK high-voltage network. SPACE WEATHER 11, 407–419.

Bloxham, J., Gubbins, D., 1988. The Evolution of the Earth's Magnetic Field. Scientific American.

Campbell, W., 1997. Introduction to Geomagnetic Fields. Vol. 1. Cambridge University Press, The Edinburgh Building, Cambridge, CB2 8RU, United Kingdom.

Carvalho, V. J. O. W. D., Hamza, V. M., Benyosef, L. C. C., 2010. Influence of Equatorial Electro Jet on Geomagnetic Field Variations in North Eastern Part of the Amazon Region (Brazil). International Journal of Geophysics and Geochemistry 2, 68–79.

Chulliat, A., Macmillan, S., Alken, P., Beggan, C., Nair, M., Hamilton, B., Woods, A., Ridley, V., Maus, S., Thomson, A., 2015. The US/UK World Magnetic Model for 2015-2020: Technical Report, National Geophysical Data Center.

Friis-Christensen, E., Lühr, H., Hulot, G., 2006. Swarm: A constellation to study the Earth's magnetic field. Earth Planets Space 58, 351–358.

Gama, L. I., 1958. Installation of the Tatuoca Magnetic Observatory. Publicações do Serviço Magnético (6).

Kearey, P., Brooks, M., Hill, I., 2002. Introduction to Geophysical Exploration. Vol. 1. Blackwell Science, Osney Mead, Oxford OX2 0EL.

Love, J., 2008. Magnetic monitoring of Earth and space. Physics Today.

Lowrie, W., 2007. Fundamentals of Geophysics, 2nd Edition. Vol. 1. Cambridge University Press, The Edinburgh Building, Cambridge, CB2 8RU, United Kingdom.

Manoj, C., Luehr, H., Maus, S., Nagarajan, N., 2006. Evidence for short spatial correlation lengths of the noontime equatorial electrojet inferred from a comparison of satellite and ground magnetic data. JOURNAL OF GEOPHYSICAL RESEARCH 111.

Matzka, J., Chulliat, A., Mandea, M., Finlay, C., Qamili, E., 2010. Geomagnetic Observations for Main Field Studies: From Ground to Space. Space Sci Rev.

Meeus, J., 1998. Astronomical Algorithms. Vol. 1. Willmann-Bell, Inc., P.O. Box 35025, Richmond, Virginia 23235.

Olsen, N., Stolle, C., 2012. Satellite Geomagnetism. Annu. Rev. Earth Planet. Sci. 40, 441–465.

Pinheiro, K., 2009. Mantle electrical conductivity estimates from geomagnetic jerk observations. Ph.D. thesis, ETH ZURICH.

Rao, P. V. S. R., Krishna, S. G., Prasad, J. V., Prasad, S. N. V. S., Prasad, D. S. V. V. D., Niranjan, K., 2009. Geomagnetic storm effects on GPS based navigation. Ann. Geophys. 27, 2101–2110.

Rasson, J. L., Toh, H., Yang, D., 2011. Geomagnetic Observations and Models, Chapter 1, The Global Geomagnetic Observatory Network. Vol. 5. Springer Science+Business Media.

Reay, S. J., Allen, W., Baillie, O., Bowe, J., Clarke, E., Lesur, V., Macmillan, S., 2005. Space weather effects on drilling accuracy in the North Sea. Annales Geophysicae 23, 3081–3088.

Silbergleit, V. M., 2015. Induced Currents in Pipelines. Scientific Research Publishing Inc. 7, 219–223.

St-Louis, B., 2011. INTERMAGNET Technical Reference Manual, Version 4.5.